Biomaterials xxx (xxxx) 123589

Contents lists available at ScienceDirect

Biomaterials

journal homepage: www.elsevier.com/locate/biomaterials

Lipid nanoparticle-mediated delivery of microRNA-124 reduces neuroinflammation

Zhanjun Ma [a, b], Hong Anh Dang [c], Jingjing Yang [a], Giulia Rodella [a], Ariane Mwema [a], Emily De Lombaerde [d], Yong Chen [d], Bruno G. De Geest [d], Vincent van Pesch [c], Giulio G. Muccioli [b, 1, *], Anne des Rieux [a, 1, **]

[a] Louvain Drug Research Institute, Advanced Drug Delivery and Biomaterials, Université Catholique de Louvain, UCLouvain, 1200, Brussels, Belgium
[b] Louvain Drug Research Institute, Bioanalysis and Pharmacology of Bioactive Lipids, Université Catholique de Louvain, UCLouvain, 1200, Brussels, Belgium
[c] Institute of Neurosciences, Neurochemistry Group, Université Catholique de Louvain, UCLouvain, 1200, Brussels, Belgium
[d] Department of Pharmaceutics, Ghent University, Ghent, 9000, Belgium

ARTICLE INFO

Keywords:
Lipid nanoparticles
Ionizable lipids
Microglia
microRNA
RNA delivery
Ionizable biscarbamate lipid
Microfluidics

ABSTRACT

MicroRNAs (miRNAs) regulate many physiological and pathological processes implicated in numerous diseases, including neuroinflammatory disorders. Chronic neuroinflammation is a key feature of neurodegenerative diseases, yet effective medications remain unavailable. Delivery of exogenous miRNAs, such as miRNA-124 (miR-124), shows promise as a therapeutic approach as it promotes microglial polarization towards an anti-inflammatory phenotype. However, the options for robust drug delivery systems to enhance miRNA mimic stability and ability to penetrate the central nervous system (CNS) are limited. Here, for the first time, we propose an LNP formulation optimized for miR-124 delivery to the CNS. We compared several ionizable lipids and selected the one that provided the highest efficiency (both regarding cell uptake, transfection efficiency and inflammation modulation) and the lowest microglia activation (S–Ac7-DOG). In cultured BV2 and primary mixed glial cells, miR-124-LNP treatment downregulated the expression of pro-inflammatory and upregulated anti-inflammatory genes. Furthermore, local delivery into the prefrontal cortex as well as intravenous injection of miR-124-LNP in lipopolysaccharides (LPS)-treated mice effectively reduced inflammation, as evidenced by the lower expression of pro-inflammatory and higher levels of anti-inflammatory cytokines. Thus, we provide a rational screening of clinically relevant LNP ionizable lipids for miRNA delivery, the demonstration of the therapeutic efficacy of miR-124-S-Ac7-DOG LNP in an LPS-induced neuroinflammation model, and finally, a non-viral, clinically translatable delivery system for miRNA therapy in the CNS. Overall, this study highlights LNP as an effective miRNA delivery vehicle for CNS applications and as a versatile platform for exploring gene therapies targeting neuroinflammation.

1. Introduction

Neuroinflammation is triggered when the central nervous system (CNS) undergoes inflammation owing to pathological processes such as infection, trauma, ischemia, autoimmunity, or exposure to toxins [1]. This process is worsened by the release of inflammatory mediators (e.g. cytokines, inflammatory enzymes, and lipids) by various immune cells, including astrocytes and microglia [2,3]. Microglia, the key CNS-resident innate immune cells in the brain, play an important role in the modulation of neuroinflammation [4]. The activation of microglia in response to pathogenic invasion or tissue injury initiates a response characterized by the secretion of pro-inflammatory cytokines, such as TNF-α, IL-1β, and IL-6 [5]. Initially, inflammatory responses are advantageous, as they facilitate tissue regeneration and eliminate cellular waste. However, if left unresolved, neuroinflammation negatively affects neuronal and oligodendroglial health, resulting in chronic tissue damage and subsequent loss of function. Dysregulated neuroinflammation has been identified as a hallmark of many neurodegenerative conditions, including traumatic injury and neurodegenerative disorders such as Alzheimer's disease and multiple sclerosis [6].

* Corresponding author.
** Corresponding author.
E-mail addresses: giulio.muccioli@uclouvain.be (G.G. Muccioli), anne.desrieux@uclouvain.be (A. des Rieux).
[1] Equal contribution.

https://doi.org/10.1016/j.biomaterials.2025.123589
Received 9 January 2025; Received in revised form 20 June 2025; Accepted 28 July 2025
0142-9612/

In recent years, RNA therapeutics have become important tools for the therapeutic arsenal. MicroRNA (miRNA) have raised a lot of interest, mostly in the context of cancer and diagnostics, but are now also being explored as therapeutic molecules. MiRNA are short endogenous single-stranded RNA of approximately 20–23 nucleotides in length that target specific mRNA at the post-transcriptional level to destabilize them or repress mRNA translation, thus regulating various biological processes, including inflammation [7]. MiRNA-124 (miR-124) is particularly abundant in the CNS and has been suggested to suppresses the activation of microglia and astrocytes [8]. MiR-124 is thought to regulate the polarization of microglia towards an anti-inflammatory/immunomodulatory phenotype (a so called "M2-like" phenotype) [9,10]. Emerging studies have demonstrated the neuroprotective effect of miR-124 in CNS diseases, such as spinal cord injury [11], Alzheimer's disease [12], and multiple sclerosis [13]. However, miRNAs have limited stability, are sensitive to nuclease degradation and are poorly internalized in cells due to their polyanionic charge. These properties hamper the broad clinical application of miRNA-based therapeutics [14].

Various vehicles have been developed to improve the efficiency and safety of RNA-based drugs and their delivery into the cytoplasm. Because of their low immunogenicity, low cytotoxicity, and up-scalable production process, lipid nanoparticles (LNP) have become one of the most clinically successful nonviral-based RNA delivery vectors [15,16]. In 2018, the first FDA-approved siRNA drug, Onpattro®, utilized LNP as a delivery vehicle, with an ionizable cationic lipid called Dlin-MC3-DMA (MC3) ensuring the electrostatic complexation of RNA as the key element of LNP stability [17]. Since then, LNP have gained widespread attention because of their role in mRNA-based COVID-19 vaccines [18]. LNP contain an ionizable cationic lipid, a "helper" phospholipid, cholesterol, and a PEGylated lipid. Each of these lipids plays a crucial role in the stability, transfection efficacy, and safety of the LNP [19]. The presence of an ionizable lipid, with low cationic charge density at neutral pH, strongly improves LNP performance, by balancing transfection efficiency and toxicity [20]. Although a few LNP formulations have been exploited to improve delivery across the blood-brain barrier (BBB) [21,22], examples of brain-targeted LNP-based RNA delivery are limited. Similarly, while the focus of LNP development has mostly been on mRNA delivery for vaccine applications and cancer therapy, few studies have addressed miRNA delivery. To the best of our knowledge, little has been done about LNP-mediated miRNA delivery for the modulation of neuroinflammation [23].

Thus, based on the properties of miR-124 and the potential of LNP, we hypothesized that LNP could be used to deliver miR-124 to the CNS to normalize neuroinflammation. MiR-124-loaded LNP were produced by microfluidics, characterized, and tested *in vitro* in LPS-activated microglia and primary mixed glial cells (MGCs). We compared six ionizable lipids and selected the lipid offering the best compromise between therapeutic efficiency and lack of microglial activation. We then demonstrated the therapeutic potential of our formulation using firstly intracerebral injection and then intravenous administration. We thus provided the proof-of-concept that S–Ac7-DOG-LNP can be used to deliver therapeutic miRNAs for the modulation of neuroinflammation (Scheme 1).

2. Material and methods

2.1. Materials

Dlin-MC3-DMA (MC3), SM102, Lipid 10, 1,2-Dioleoyl-*sn*-glycero-3-phosphoethanolamine (DOPE), DSPE-PEG2000, 3-[4,5-dimethylthiazol-2-yl]-2,5 diphenyl tetrazolium bromide (MTT), Amiloride hydrochloride (Amil), Genistein (Gen), Methyl-β-cyclodextrin (mβCD), and Bafilomycin A1 (Baf A1) were purchased from Med Chem Express EU (MCE, Sweden). ssPalmO-Phe (SS-OP) and C12-200 were obtained from Cayman (Michigan, USA). S–Ac7-DOG was synthesized according to literature [24]. Dulbecco's Modified Eagle Medium (DMEM), DMEM + GlutaMAX™, Opti-MEM, Dulbecco's phosphate buffered saline (DPBS), Hanks' Balanced Salt Solution (HBSS), Trizol, Penicillin-Streptomycin (P/S), Chlorpromazine hydrochloride (CPZ), Hoechst 33342, Lipofectamine™ 3000 Transfection Regent (L3K), Slide-A-Lyzer™ G3 Dialysis Cassettes (10K), and Quant-iT RiboGreen RNA Assay kit were purchased from Thermo Fisher Scientific® (Waltham, MA). 1,2-distearoyl-*sn*-glycero-3-phosphocholine (DSPC), DMG-PEG2000, Cholesterol, Fetal Bovine Serum (FBS), LPS from *E. coli* (serotype O55:B5), poly-D-Lysine, Triton™ X-100, and DAPI were purchased from Sigma-Aldrich (Merck, Germany). Anti-Luciferase (Luc) siRNA and Cy5-labeled miR-124-3p mimic were purchased from Horizon Discovery (Waterbeach, UK). QIAzol lysis reagent, miRCURY LNA mimics for miR-124-3p, miR-124-5p, and negative control (NC), miR-103a-3p primer, and miR-124-3p primer were purchased from Qiagen (Hilden, Germany). mRNA primers were purchased from Integrated D.N.A. technologies (Leuven, Belgium). Rotilabo®-syringe filters of 0.22 μm, paraformaldehyde (PFA), and Dimethyl sulfoxide (DMSO) were purchased from Carl Roth GmbH (Germany).

2.2. LNP formulation

RNA-LNP were produced by rapid mixing of an ethanolic solution containing ionizable lipids, cholesterol, DOPE, and DSPE-PEG2000 at a molar ratio of 50:38.5:10:1.5 with an aqueous solution of RNA in 25 mM acetate buffer at pH 4.0, using a NanoAssemblr Ignite® microfluidic mixing device (Precision Nanosystems Inc.) at a 1:3 (vol: vol) ratio and a total flow rate of 15 mL/min. The total lipid concentrations were 6 and 8 mM and N/P (N: mole of ionizable cationic nitrogen atoms in the ionizable lipid; P: mole of anionic phosphates in RNAs) ratio of 6 and 10 were tested. RNA-LNP were then dialyzed against a 500-fold volume of PBS (pH 7.4) for 24 h to remove residual ethanol (Float-A-Lyzer dialysis cassette, 10 kDa) and then filter-sterilized (0.2 μm) and stored at 4 °C. When required (for *in vivo* experiments), miRNA-LNP were concentrated using Amicon® Ultra 3 K centrifugal filter units (Merck Millipore Ltd., USA).

2.3. LNP characterization

LNP were diluted 50-fold with 1 × PBS for the measure of size, polydispersity index (PDI) and with double-distilled water (pH 7.4) for zeta potential measurement, respectively, via dynamic light scattering (DLS) (Zetasizer Nano ZS, Malvern, UK). RNA encapsulation efficiency was measured using a Quanti-it™ RiboGreen RNA assay kit, according to the supplier instructions. The RNA-LNP suspension was either diluted with TE buffer (measuring unencapsulated RNA) or with 1 % Triton X-100 in TE buffer (measuring total RNA). The RiboGreen reagent was added, and the fluorescence was measured using a multimode microplate reader (Molecular Devices Spectramax® iD5, California, USA) at λ_{ex} = 480 nm and λ_{em} = 520 nm. Encapsulation efficiency (EE%) was calculated as follows: EE% = ((1- unencapsulated RNA)/total RNA) × 100 %.

2.4. Cell culture

BV2 cells (a mouse microglial cell line) and Luciferase (Luc)-expressing BV2 (Luc-BV2) cells (transduced by Prof. Thomas Michiels' team, de Duve Institute, UCLouvain) stably modified to express firefly Luc were maintained in high glucose DMEM supplemented with 10 % FBS, 1 % (v/v) penicillin, and 1 % (v/v) streptomycin [25]. Primary cortical mixed glial cells (MGCs) were extracted from Sprague-Dawley rat pups (postnatal days 1–2) according to previous report [26,27]. Briefly, brains were dissected, cerebellum, olfactory bulbs, and meninges were removed. Brains were then digested using papain

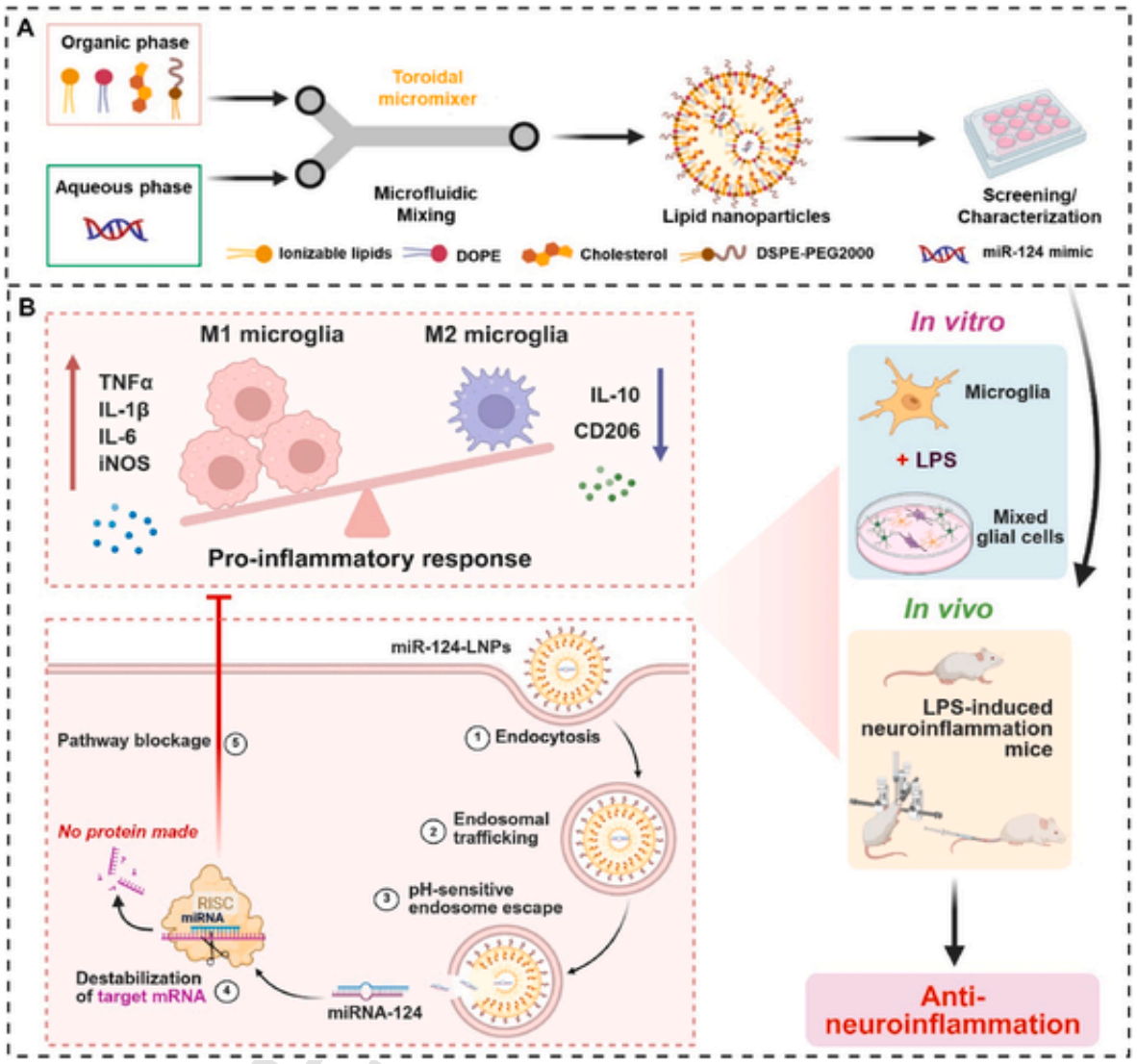

Scheme 1. Schematic illustration of miR-124-LNP for suppressing neuroinflammation. A. Preparation of miR-124-LNP containing different ionizable lipids using a microfluidic method. **B**. Schematic showing the therapeutic efficacy of miR-124-LNP in LPS-induced neuroinflammation *in vitro* and *in vivo*. Modified icons from BioRender.com.

(40 μg/mL) and slowly dissociated mechanically using a G18 and a G23 syringe needles. The cell suspension was diluted in DMEM medium (4.5 g/L glucose, L-glutamine, pyruvate, 10 % FBS (v/v) and 1 % P/S (v/v)) then filtered through a 40 μm cell strainer. Then, the MGCs were cultured up to 8 days and used for treatment. All cells were kept in an incubator set at 37 °C with 5 % CO_2 and a relative humidity of 95 %.

2.5. LNP in vitro cytotoxicity

A MTT assay was used to evaluate the *in vitro* cytotoxicity of the different LNP formulations using BV2 cells and MGCs. Briefly, BV2 cells were seeded at a density of 6×10^3 cells per well in 96-well plates and incubated overnight for adherence. MGCs were plated at 1.68×10^5 cells/well in poly-D-Lysine coated (1 μg/mL) 96-well plates and incubated for 8 days before use. Next, different concentrations of LNP were added on cells to achieve a final volume of 100 μL per well. After 24 h incubation at 37 °C, 10 μL of MTT (5 mg/mL) was added to each well, followed by incubation for a further 4 h. Then, the medium was removed and the absorbance was measured using a multimode microplate reader at 570 nm after 100 μL DMSO was applied to dissolve the purple formazan crystals. Untreated cells were used as positive control (100 % viability).

2.6. Luciferase knockdown assay

Luc-BV2 cells were seeded in 96-well plates at a density of 1×10^4 per well and incubated overnight. Cells were then treated with the different LNP loaded with siRNA targeting Luc at different doses (5, 10, 20, 40, and 80 nM diluted in 100 μL of Opti-MEM). After 24 h of incubation, 100 μL of ONE-Glo™ Luciferase Assay solution (Promega, Madison, WI) was added to each well. After 10 min, luminescence was measured with a microplate reader to quantify luciferase activity.

2.7. Cellular uptake of LNP by microglial cells

BV2 cells were seeded in 24-well plates at a density of 20×10^4 cells per well. The next day, cells were treated with Cy5-miRNA-loaded LNP in Opti-MEM™ medium at an equivalent concentration of 40 nM of miRNA and incubated at 37 °C for 6 h. The cells were washed three times with ice-cold PBS, harvested and resuspended

in 0.5 mL of PBS. The uptake of miRNA by BV2 cells was quantified by flow cytometry (CYTEK Aurora, USA).

To visualize the intracellular distribution of Cy5-miRNA-loaded LNP, confocal laser scanning microscopy was used to track the location of the Cy5 signal within microglial cells. BV2 cells were seeded overnight on μ-slide 8-well chamber slides (Ibidi GmbH, Germany) (6×10^4 cells per well). The LNP containing Cy5-labeled miRNA were incubated with the cells (40 nM of miRNA) for 6 h at 37 °C. Next, the cells were washed twice with PBS, fixed with 4 % (w/v) PFA for 30 min at room temperature (RT), and washed again before staining of cell membrane with iFluor® 488-Wheat Germ Agglutinin (WGA, 10 μg/mL, AAT Bioquest, USA) and cell nuclei with DAPI (1 μg/mL). Image acquisition was performed using a high-throughput confocal laser scanning microscopy (Zeiss Spinning disk confocal COSD, Germany).

2.8. LNP uptake mechanism

Different inhibitors of endocytosis were employed to investigate the uptake mechanism of LNP. BV2 cells were seeded overnight on μ-slide 8-well chamber slides (6×10^4 cells per well). Then, cells were preincubated for 1 h with Amil (100 μM), Gen (300 μM), CPZ (10 μM), MβCD (5 mM) at 37 °C or were incubated at 4 °C, respectively [28,29]. Cells incubated without inhibitors were used as a positive control. Then, Cy5-miRNA-loaded LNP were added for 6 h before measure of the Cy5 intensity in cells by flow cytometry (CYTEK Aurora, USA).

The endosomal entrapment and escape of miR-LNP were observed by a high-throughput confocal laser scanning microscope. Briefly, BV2 cells were seeded in a μ-slide 8-well chamber slide at a density of 6×10^4 cells/well and cultured overnight. Then, the cells were treated with Cy5-labeled LNP for 1 h, 3 h, and 6 h. After incubation, the endosomes and lysosomes were stained with LysoBrite™ Green (1:500 in PBS, AAT Bioquest, USA) for 30 min at 37 °C. Hoechst 33342 (1 μg/mL) was used to stain the nuclei and cells were imaged using confocal laser scanning microscopy (Multiphoton Laser Scanning Microscopy, LSM 980, Zeiss, Germany) and analyzed by image J.

2.9. Inflammatory cytokine expression of glial cells

BV2 cells and primary MGCs were used to assess the transfection efficiency of miR-124-LNP *in vitro*. BV2 cells were seeded in 24-well plate at the initial density of 10×10^4 cells per well in culture medium and cultured overnight. MGCs were plated at 100×10^4 cells per well in poly-D-Lysine coated (1 μg/mL) 24-well plate for 8 days. Then, cells were treated for 24h with miR-124 and miR-negative control (miR–NC) –loaded LNP at a final concentration of 40 nM of mimics. L3K in Opti-Mem medium was used as control, according to the manufacturer's instructions. Then, cells were incubated for 8 h with LPS (100 ng/mL) [30]. The medium was removed and Trizol or QIAzol was added on the cells before storing at −80 °C for subsequent analysis by Reverse Transcriptase Quantitative Polymerase Chain Reaction (RT-qPCR).

2.10. mRNA extraction and RT-qPCR

Total RNA was extracted from cells or tissues using the Trizol reagent according to the manufacturer's instructions. MiRNA was extracted with QIAzol lysis reagent following the miRNeasy Mini Kit protocol with RPE and RWT buffer (Qiagen) combined with Enzymax RNA Mini spin columns (Enzymax, USA). Total RNA concentration was measured on a Nanodrop 2000 spectrophotometer (Thermo Scientific, USA), and cDNA was synthesized using the GoScript reverse transcription kit (Promega) from 1 μg of total RNA.

MiRNA were reverse transcribed from 100 ng of RNA using miRCURY LNA RT (Qiagen). qPCR was performed using the GoTaq qPCR Master Mix (Promega) for mRNA and miRCURY LNA SYBR Green PCR kit (Qiagen) for miRNA, on a QIAquant 96 2plex (230 V) instrument and software (Qiagen). Relative gene expression changes were calculated using the $2^{-\Delta\Delta CT}$ method. Values were normalized to expression levels of 60S ribosomal protein L19 (RPL19) (mouse) or RPL13 (rat) for the mRNA and miR-103a-3p for the miRNA. Primers sequences for qPCR are listed in Table S1 and Table S2.

2.11. In vivo model of neuroinflammation

All experiments were performed following the Belgian national regulation guidelines and following EU Directive 2010/63/EU and were approved by the ethical committee for animal care of the Faculty of Medicine of the Université catholique de Louvain (2024/UCL/MD010; 2024/UCL/MD066; 2025/UCL/MD057). Mice were housed in filter-top cages under artificial light (12-h dark/12-h light) and controlled conditions of temperature (20–22 °C) and had free access to food and drinking water.

2.11.1. MiR-124-3p transfection efficiency

Female Swiss mice (6 weeks old, Janvier) were used to study the miR-124-3p expression after treatment with miR-LNP, formulated with either Dog or MC3 ionized lipids. MiR-124-Dog-LNP and miR-124-MC3-LNP containing 5 μg of miR-124 were injected intramuscularly in the right quadriceps femoris of mice. The mice were euthanized 24 h later and the right quadriceps were collected. MiR-124-3p and cytokine mRNA expression were analyzed by RT-qPCR as described in 2.10.

2.11.2. Inflammatory marker gene expression

To induce neuroinflammation in mice, 5 mg/kg of LPS in saline was injected intraperitoneally (i.p.) to female Swiss mice (6 weeks, Janvier) [31,32]. Regarding the intracerebral (i.c.) administration, after 1 h of LPS, mice were divided into 4 groups: PBS-treated mice, LPS-treated mice (LPS + PBS), LPS and LNP-miR-NC (0.8 μg/mouse)-treated mice, and LPS and LNP-miR-124-3p (0.8 μg/mouse) treated mice. Injection of PBS or LNP was performed by i.c. administration in the prefrontal cortex of mice using convection-enhanced delivery. Firstly, mice were anesthetized by i.p. injection of ketamine/xylazine (100 and 13 mg/kg, respectively) and lidocaine (10 mg/mL, 30 μL/incision) was administered at the surgery site before making a skin incision on the top of the skull. Anesthetized animals were fixed on a stereotaxic frame and were injected with 0.8 μg of miR encapsulated into LNP (or vehicle) using a Hamilton syringe (10 μL, 26S gauge needle) mounted on an infusion syringe pump (Harvard Apparatus, Holliston, MA, USA). A total volume of 4.5 μL was injected by 3 subsequent injections in the prefrontal cortex (−1 mm medial/lateral; +1.9 mm anterior/posterior; 2.6, 2.0, and 1.4 mm depth below brain surface; 1.5 μL of LNP per injection site) at a rate of 0.5 μL/min [33,34]. The needle was left for 1 min after injection to avoid reflux. Regarding the intravenous (i.v.) administration, after 1 h of LPS, mice were divided into 4 groups: PBS-treated mice, LPS-treated mice (LPS + PBS), LPS and LNP-miR-NC (1 mg/kg)-treated mice, and LPS and LNP-miR-124-3p (1 mg/kg) treated mice. The mice were injected via the lateral tail vein with PBS or LNPs (150 μL) at 1 h and 9 h for a total of 2 doses. After 24 h, mice received an anesthetic overdose and were euthanized by decapitation. Prefrontal cortexes at the site of injection were rapidly dissected and then stored at −80 °C until RT-qPCR analysis.

2.12. Statistical analysis

The data are presented as mean ± standard deviation (SD) ($n \geq 3$). Data analysis were performed using GraphPad Prism 9 software (GraphPad, San Diego, CA, USA). One-way analysis of variance (ANOVA) with Tukey's correction (for multiple comparisons) and Student's *t*-test (between two groups) were used to calculate statistical significance. Significance marks were categorized with the following *p*-values: $*p < 0.05$, $**p < 0.01$, $***p < 0.001$, $****p < 0.0001$.

3. Results

3.1. Selection of miR-124-3p as an anti-inflammatory miRNA

First, we investigated the effects of miR-124 transfection on LPS-mediated microglial activation. For this, we compared the effects of both strands of miR124, namely miR-124-3p and miR-124-5p, on LPS-activated BV2 cells. BV-2 cells were transfected, using Lipofectamine™ 3000 Transfection Reagent (L3K), with either a scramble miR (miR-NC, negative control), miR-124-5p or miR-124-3p mimics for 24 h followed by exposure to LPS for 8 h. LPS treatment resulted in a significant increase in M1-like marker (e.g. TNF-α, IL-1β, iNOS) gene expression by BV2 cells. Transfection with miR-124-5p or miR-124-3p decreased the LPS-mediated increase in mRNA expression of these markers (Fig. 1A–E). Additionally, there was a substantial increase in the expression of the M2-like markers IL-10 and CD206 when cells were transfected with miR-124-3p, but not with miR-124-5p (Fig. 1F–G). Thus, while both miR-124-3p and miR-124-5p decreased the gene expression of pro-inflammatory markers, only miR-124-3p increased the gene expression of anti-inflammatory cytokines and was therefore selected for further experiments (and will be referred as miR-124 from now on).

Bioinformatics analyses (TargetScan, Starbase, and miRDB) suggested that binding sites for miR-124 are located in the 3′-UTR of the phosphodiesterase 4B (PDE4B) and tumor necrosis factor receptor-associated factor 6 (TRAF6) mRNA, making PDE4B and TRAF6 two potential targets for miR-124 (Fig. 1H). To confirm the effects of miR-124 on PDE4B and TRAF6 in our model, BV2 cells were transfected with miR-NC and miR-124 mimics for 24 h. A significant reduction of PDE4B and TRAF6 mRNA levels was observed after transfection with miR-124 (Fig. S1). Similarly, miR-124 repressed PDE4B and TRAF6 expression in LPS-stimulated BV2 cells (Fig. 1I–J).

3.2. Optimization of miR-LNP production by microfluidics

MiR–NC–LNP were formulated by mixing an aqueous phase containing miR-NC and an organic phase containing MC3 (ionizable lipid), DOPE (helper lipid), cholesterol (helper lipid), and DSPE-PEG2000 (PE-Gylated lipid) using the Ignite® instrument (Fig. 2A) as described for

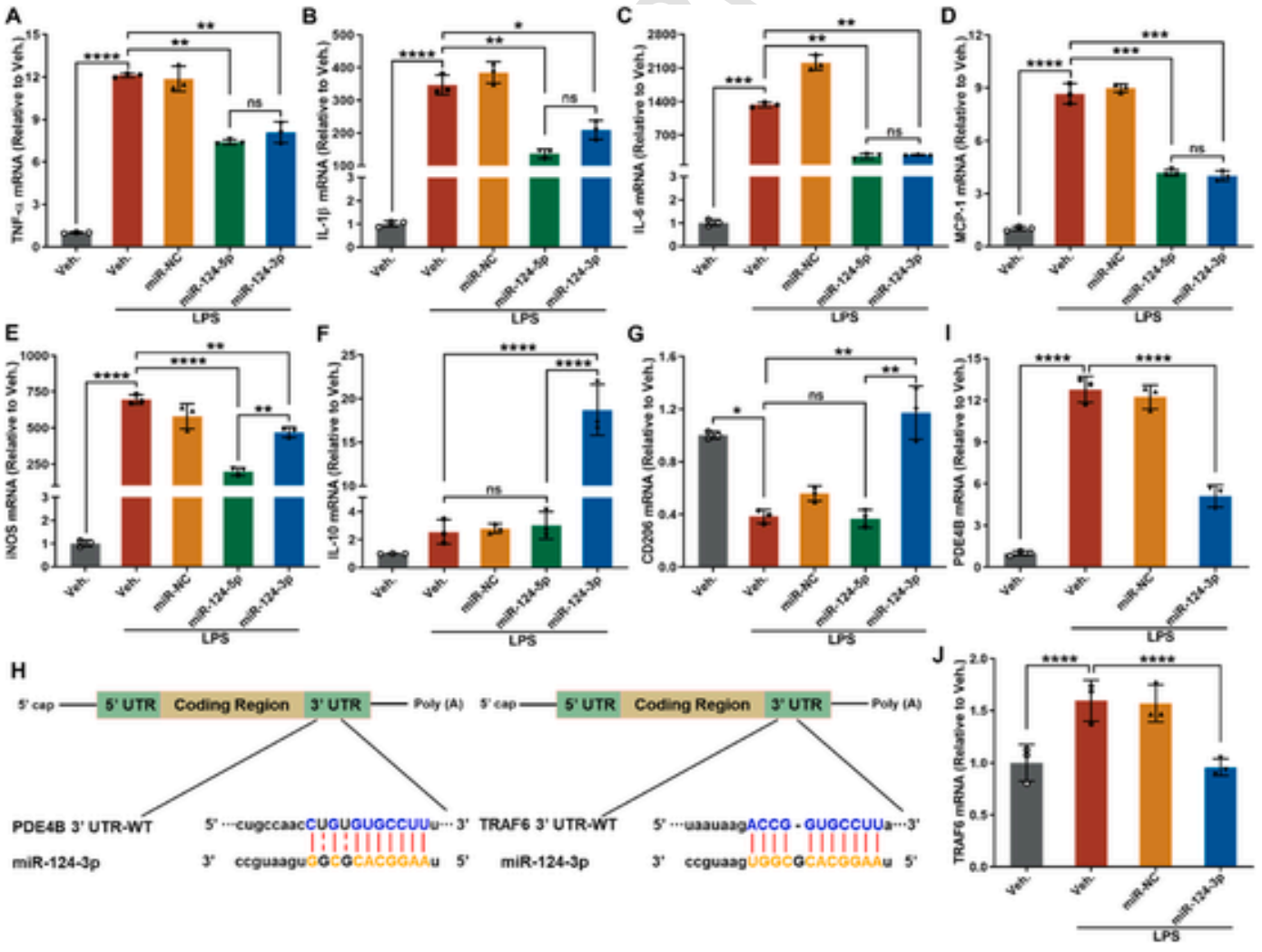

Fig. 1. MiR-124-3p inhibited LPS-induced inflammatory response in microglial BV2 cells **A-G**. BV2 cells were transfected with miR-negative control (miR-NC), miR-124-5p, or miR-124-3p mimics for 24 h, followed by 8 h treatment with LPS (100 ng/mL). The mRNA levels of the pro-inflammatory markers TNF-α (**A**), IL-1β (**B**), IL-6 (**C**), MCP-1(**D**), and iNOS (**E**), as well as of the anti-inflammatory markers IL-10 (**F**) and CD206 (**G**) were quantified using RT-qPCR. **H**. Bioinformatics was used to predict the binding sites between miR-124-3p and 3′-UTR of PDE4B and TRAF6. **I-J**. Expression of PDE4B and TRAF6 mRNA after transfection with miR-NC or miR-124-3p mimics for 24 h followed by 8 h LPS. Data are presented as mean ± SD (N = 3, n = 3); *$P < 0.05$, **$P < 0.01$, ***$P < 0.001$, ****$P < 0.0001$, ns, not significant, $P > 0.05$.

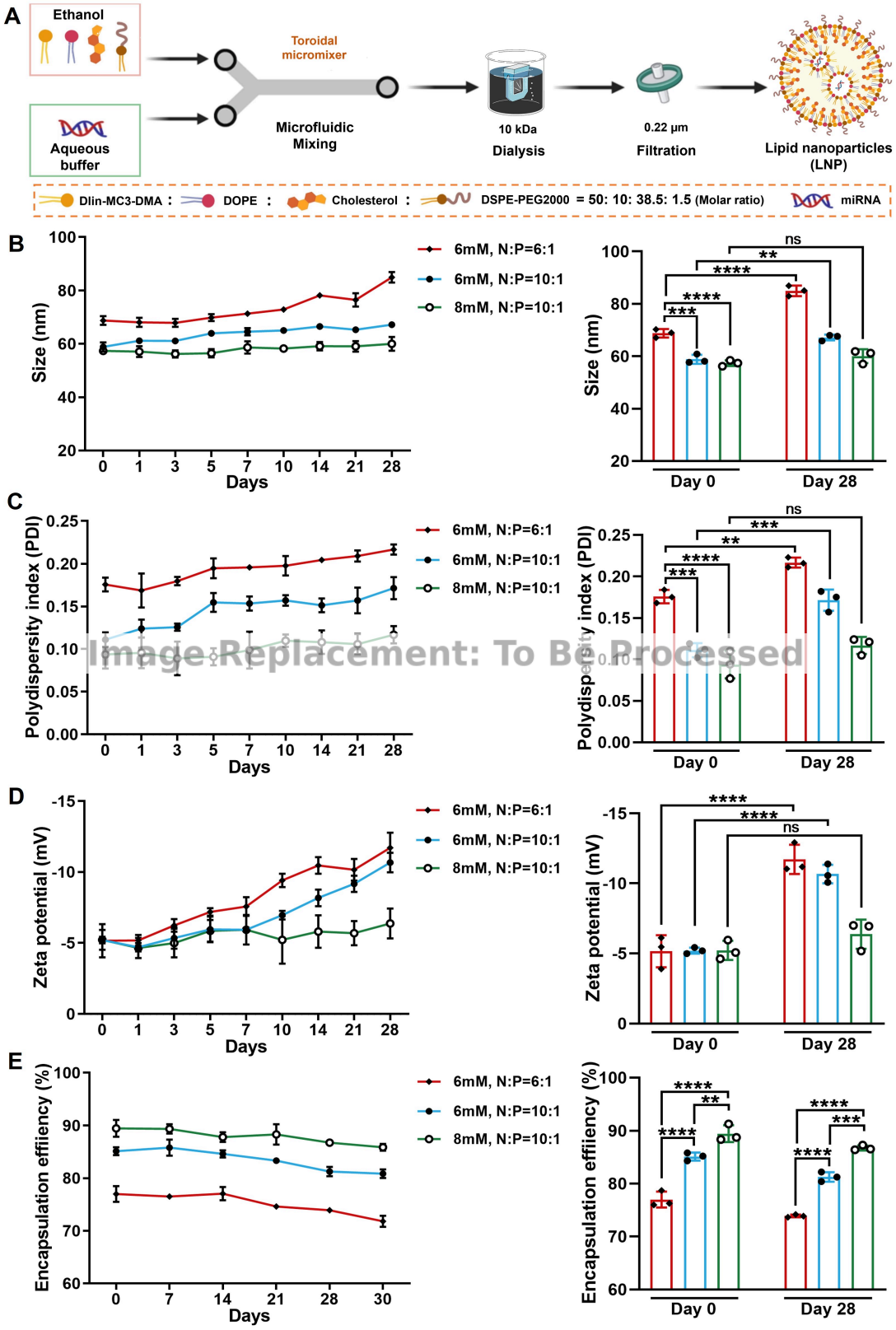

Fig. 2. Optimization of miR-LNP production by microfluidics **A.** Schematic diagram of miR-LNP production via rapid mixing through a toroidal microfluidic chip (Ignite® instrument, Precision Nanosystem™). LNP were formulated by diluting miRNA in an aqueous buffer and mixing the organic and aqueous phases to promote LNP self-assembly. **B-D**. The size, PDI, and zeta potential of different miR-LNP were evaluated using DLS. **E**. Percentage of encapsulation efficiency (EE) of LNP as

Fig. 2.—*continued*
measured by a RiboGreen assay. The data were represented as mean ± SD (N = 3); *$P < 0.05$, **$P < 0.01$, ***$P < 0.001$, ****$P < 0.0001$, ns, not significant, $P > 0.05$.

mRNA encapsulation by Gimondi et al. [35]. The lipids MC3, cholesterol, DOPE, and DSPE-PEG 2000 were combined at a molar ratio of 50:38.5:10:1.5, which is the commonly used ratio for LNP formulation, notably used for the mRNA-based COVID-19 vaccines [16]. The total lipid concentration as well as the ratio of ionizable lipids to RNA (N:P) can impact LNP physicochemical properties and stability [15]. Different N:P ratio (6:1 and 10:1) and different lipid concentrations (6 mM and 8 mM) were thus tested.

The obtained LNP had a size between 58 and 69 nm, a polydispersity index (PDI) between 0.09 and 0.18 and a zeta potential of around −5 mV (Fig. 2B–D). The encapsulation efficiency (EE) of the miRNA varied between 77 % and 89 % (Fig. 2E). The stability of the different formulations at 4 °C was evaluated over four weeks by measuring the size, PDI, zeta potential, and miRNA EE. A total lipid concentration of 8 mM combined with a N:P ratio of 10:1 gave the smallest size and PDI, and the highest EE. The zeta potential of these LNP was also more stable over time. Based on these results, a total lipid concentration of 8 mM and a N:P ratio of 10:1 were selected for the miRNA-loaded LNP formulations.

3.3. Screening and characterization of LNP for efficient delivery to microglial cells

The ionizable lipid is the key component of the LNP formulation, and its apparent acid dissociation constant (pKa) determines the ionization behavior and surface charge density of LNP, which further affects their stability and endosomal escape [20]. Thus, six different ionizable lipids were tested to determine which one(s) would provide the best compromise between cell viability, microglial activation, and siRNA transfection. Dlin-MC3-DMA (MC3) and SM102 lipids are approved by the FDA as part of Onpattro® and Moderna®. C12-200 is a branched-chain ionizable lipid with five hydroxyl groups, that is widely used for vaccine applications. S–Ac7-DOG (Dog), ssPamlO-Phe (SS-OP), and Lipid 10 were recently developed as biodegradable ionizable lipids and are described to exhibit a higher endosome escape efficiency. Besides the ionizable lipid, we selected DOPE as the helper lipid and DSPE-PEG as the PEGylated lipid based on the literature. DOPE was reported to be more efficient than DSPC in eliciting endosomal escape [36]. DSPE-PEG is known to stabilize the LNP, providing longer circulation times and a lower accumulation in the liver compared to DMG-PEG [37]. DSPE-PEG is part of the Doxil® formulation, so it is also FDA approved. Thus, LNP containing DOPE, DSPE-PEG, cholesterol and MC3, SM102, C12-200, Dog, SS-OP, and Lipid 10 as their ionizable lipid (Fig. 3) were formulated to encapsulate a siRNA against luciferase (Luc), allowing for a quick and straightforward assessment of luciferase silencing efficiency using luciferase-expressing BV2 cells.

The different LNP formulations featured hydrodynamic diameters between 60 and 76 nm, PDI values between 0.03 and 0.12 and zeta potential values between −0.5 and −6.8 mV (Fig. 4A–C). The EE was similarly high in all LNP formulations (>80 %) except for the SS-OP LNP for which the EE was slightly lower (74.5 %) (Fig. 4D). No significant differences were observed between formulations. LNP size, PDI, Zeta potential, and EE were stable for 30 days at 4 °C whatever the ionizable lipid used (Fig. S2).

Besides LNP physico-chemical characteristics, cytotoxicity, microglial activation and transcription efficiency were important parameters to evaluate in the formulation selection process. Here, cell viability was not affected when BV2 cells were incubated with the formulations, except for SM-102-LNP and C12-200-LNP (from 20 nM upward), which induced a dose-dependent cytotoxicity (Fig. 4E). To eliminate formulations that could potentially activate microglial cells, the different LNP were incubated with BV2 cells, and their impact on the expression of pro-inflammatory markers was evaluated. Only LNP-containing the lipid C12-200 increased proinflammatory markers mRNA compared to the vehicle (Fig. 4F–J).

Then, the silencing efficiency of the 6 anti-Luc siRNA-loaded formulations was tested by measuring the bioluminescence of Luc-BV2 cells. All formulations were able to efficiently silence Luc, albeit at different concentrations depending on the ionizable lipid used (Fig. 4K). C12-200-LNP provided the highest silencing efficiency but induced BV2 cell activation, hence, it was not selected for further experiments. At the miRNA dose usually reported for *in vitro* experiments (i.e. 40 nM), all the formulations induced comparable gene silencing. So, SS-OP, Dog,

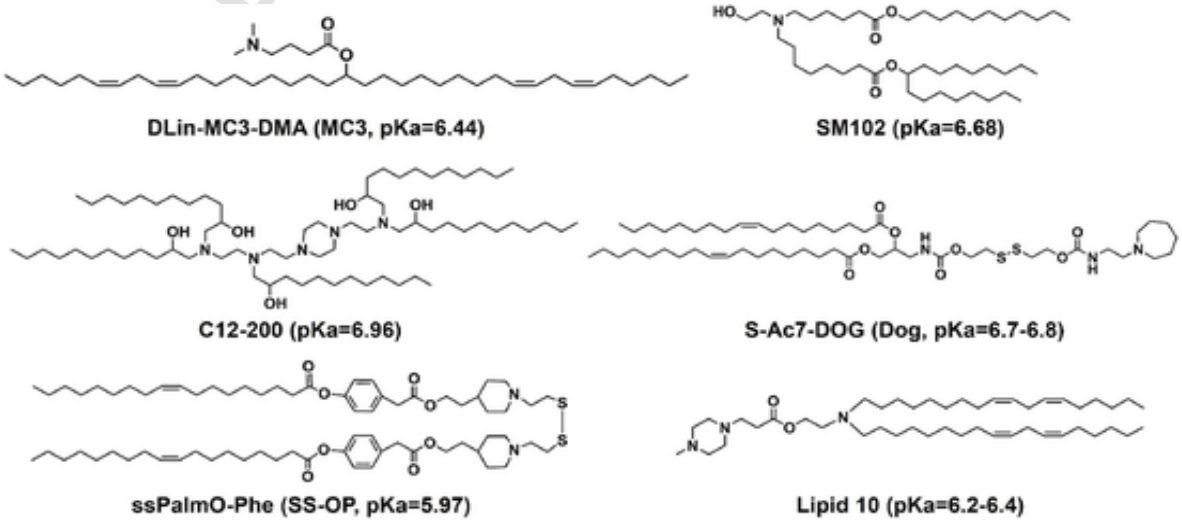

Fig. 3. Ionizable lipids used in the formulation of LNP Structure and pKa value of MC3, SM102, C12-200, Dog, SS-OP, and Lipid 10 that were used as ionizable lipids in the LNP formulation.

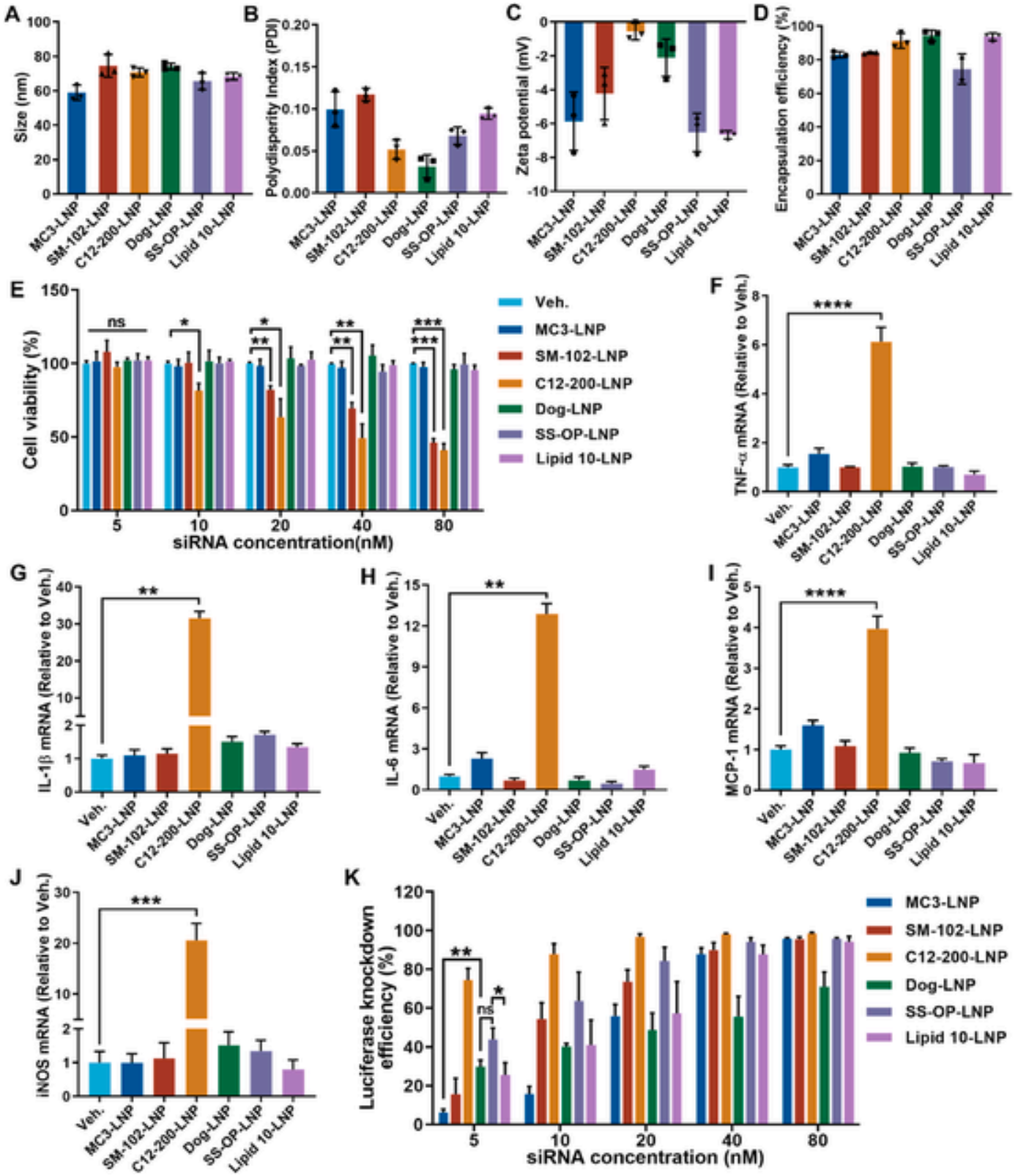

Fig. 4. Screening of ionizable cationic lipids for the transfection microglial cells **A.** LNP mean size (nm); **B**. PDI. **C**. Zeta potential (mV), as measured using a Zeta-Sizer (N = 3). **D**. EE of LNP (N = 3). **E**. Cell viability of BV2-Luc cells treated with different doses of siLuc (5, 10, 20, 40, and 80 nM) for 24 h using different LNP formulations (N = 4, n = 5); **F-J**. The relative mRNA expression levels of TNF-α, IL-1β, IL-6, MCP-1, and iNOS in BV2-Luc cells (N = 3, n = 4). **K**. Average lu-

Fig. 4.—*continued*
ciferase knockdown efficiency in BV2-Luc cells treated with various LNP at 5, 10, 20, 40, and 80 nM siLuc concentration for 24 h (N = 4, n = 4). Data are presented as mean ± SD; *$P < 0.05$, **$P < 0.01$, ***$P < 0.001$, ****$P < 0.0001$, ns, not significant, $P > 0.05$.

MC3, and Lipid 10 were selected for the assessment of miR-124 encapsulation.

3.4. Impact of ionizable lipids on miR-LNP delivery to microglial cells

The 4 ionizable lipids selected (*i.e.*, MC3, Dog, SS-OP and Lipid 10) were then used to formulate miR-124-containing LNP (miR-124-LNP). MiR-124-loaded LNP featured the same physicochemical characteristics than siLuc-loaded LNP (Fig. 5A–D). On average, the same number of siRNA and miRNA molecules were loaded in LNP (1.46 and 1.50 nmoles, respectively). MiR-124-LNP size was between 57 and 72 nm, their PDI between 0.07 and 0.13, and their zeta potential between −4 and 8 mV (Fig. Fig. 5A–D). The EE of miRNA was similar for all formulations (>85 %). MiR–NC–LNP presented the same properties than miR-124-LNP (Table S3).

To assess the impact of the ionizable lipid on LNP uptake by microglial cells, Cy5-labeled miR-124 was encapsulated in the different LNP. The formulations showed the same characteristics than miR-124-loaded LNP (Table S4). BV2 cells were then incubated with Cy5-miR-124-LNP and Cy5-miR-124 mixed with lipofectamine (miR-124-L3K) as control) for 6 h. The cellular uptake was visualized by confocal microscopy and quantified by FACS.

A higher fluorescence intensity was observed for all formulations, including L3K, compared to unformulated Cy5-miRNA (Fig. 5E). A quantitative comparison was performed using flow cytometry after 3 h and 6 h of incubation to confirm these observations. Dog-LNP and SS-OP-LNP showed the highest fluorescence intensities compared to L3K and the other LNP (Fig. S3; Fig. 5F–G).

BV2 cells were incubated with the different miR-124-LNP for 24 h and the relative level of miR-124 was quantified. All formulations resulted in increased level of miR-124 compared to the respective miR-NC control, with Dog-LNP providing the highest miR-124 level compared to the other LNP and L3K (Fig. 6).

Based on these results, S–Ac7-DOG (Dog) lipid was selected as the ionizable lipid for the miR-124 formulation for subsequent experiments.

3.5. Uptake mechanism and endosomal escape of miR-S-Ac7-DOG-LNP

Achieving efficient cell entry is essential for miRNA delivery. To better understand the mechanism of S–Ac7-DOG-LNP cellular uptake, endocytic inhibitors Amil (macropinocytosis), Gen (caveolin-mediated endocytosis), CPZ (clathrin-mediated endocytosis), and MβCD (surface cholesterol depletion) [28] or incubation at 4 °C (energy-dependent endocytosis) were used in combination with Cy5-miR-124-LNP. The cellular association of Cy5-miR-LNP was significantly decreased at 4 °C in BV2 cells, suggesting that its internalization pathway is mediated by energy-dependent endocytosis (Fig. 7A–B). When cells were pretreated with MβCD, LNP internalization was also almost totally inhibited while it was significantly reduced in presence of CPZ (93.9 % and 20.4 %, respectively). In contrast, Amil and Gen barely affected LNP uptake. These results suggested that S–Ac7-DOG-LNP were internalized by an endocytosis pathway by BV2 cells where cholesterol is required.

Rapid escape of miRNA from endosomes and lysosomes to the cytosol is important for an efficient gene silencing [38]. To further probe the intracellular fate of internalized miR-S-Ac7-DOG-LNP, intracellular trafficking of Cy5-miRNA-LNP was monitored by confocal microscopy to investigate their ability for endosomal escape. Hoechst 33342 and LysoBrite™ Green were used to stain the cell nuclei and acidic compartments (*i.e.*, late endosomes and lysosomes), respectively. The lesser the colocalization of lysosomes and Cy5-miR-LNP, the more effective the endosomal escape. Our results suggest that the overlap between the red fluorescence of Cy5 and the green fluorescence of LysoBrite gradually decreased as the incubation time was prolonged, hinting at the successful escape of the LNPs from endo/lysosomes (Fig. 7C). Baf A1 was used to further explore the intracellular trafficking mechanism of miR-124-Dog-LNP. Baf A1 is a well-known proton pump inhibitor that selectively inhibits vacuolar H^+-adenosine triphosphatase (V-ATPase) and as such would disturb endocytosis and intracellular trafficking, including endosomal escape [39]. Baf A1 treatment significantly decreased the accumulation of Cy5-miR-124 in BV2 cells (72.7 % decrease) (Fig. 7D–E).

3.6. Impact of miR-124-S-Ac7-DOG-LNP on inflammation markers in microglial cells

To investigate the anti-inflammatory potential of miR-124-S-Ac7-DOG-LNP, its impact on the expression of inflammation marker genes in LPS-activated BV2 cells was evaluated (Fig. 8A). LPS treatment led to a marked increase in PDE4B, TRAF6, and pro-inflammatory cytokine expression (TNF-α, IL-1β, IL-6, MCP-1, and iNOS) (Fig. 8B–H). Both miR-124-LNP and miR-124-L3K significantly reduced the expression levels of PDE4B, TRAF6, TNF-α, IL-1β, IL-6, MCP-1, and iNOS. The expression of M2-like markers (IL-10 and CD206) was significantly enhanced by miR-124-LNP and miR-124-L3K (Fig. 8I–J). Meanwhile, both miR-124-LNP and miR-124-L3K significantly increased the ratio of CD206/iNOS (M2/M1 markers) compared to the LPS group (Fig. S4). Delivery of miR-124 with LNP and L3K had the same effect, but the viability of BV2 cells exposed to the L3K transfection agent was significantly lower compared to LNP (by 50 %) (Fig. 8K).

3.7. Impact of miR-124-S-Ac7-DOG-LNP on inflammation markers in MGC

Next, we wanted to confirm the anti-inflammatory efficiency of miR-124-LNP in a more complex *in vitro* system using a mixed-culture system (MGC) consisting of primary microglia, astrocytes, oligodendrocytes and oligodendrocyte progenitor cells [26]. Primary MGC were isolated from the cortex tissue of the brain of Sprague-Dawley newborn rats (Fig. 9A). No significant cytotoxicity was observed when the cells were treated with miR-124-LNP at different concentrations (Fig. S5). Next, the levels of miR-124 were assessed following increasing incubation times (Fig. S6A). The levels miR-124 in the cells treated with miR-124-S-Ac7-DOG-LNP were increased (compared to (miR–NC–LNP-treated cells) after only 1 h of incubation and did not increase further when the incubation time was longer (up to 24 h). However, a significant reduction of PDE4B and TRAF6 mRNA expression was observed after 24 h (Fig. S6B) and 12 h, respectively (Fig. S6C). Thus, the efficacy of miR-124-LNP in modulating the expression of inflammatory markers in MGC was assessed 24 h after exposure to LNP. MiR-124-LNP significantly reduced the mRNA expression of PDE4B, TRAF6, TNF-α, IL-1β, IL-6, MCP-1 and iNOS to a similar extent as the positive control (miR-124-L3K), compared to miR-NC (Fig. 9B–H). Coincidentally, miR-124-LNP increased IL-10 expression compared to miR–NC–LNP, untreated activated MGC and miR-124-L3K (Fig. 9I). The level of CD206 gene expression was significantly increased in LPS-stimulated MGC after treatment with miR-124-LNP and miR-124-L3K compared to controls (Fig. 9J). MiR-124-LNP and miR-124-L3K significantly increased the ratio of CD206/iNOS (M2/M1-like ratio) compared to the vehicle-treated LPS condition, while miR-124-LNP induced a higher ratio compared to miR-124-L3K-treated cells (Fig. S7). Additionally, Dog-LNP seemed to show a better efficiency compared to “gold standard” formulations, namely FDA-approved Onpattro® and Moderna® -like LNP (Fig. S8).

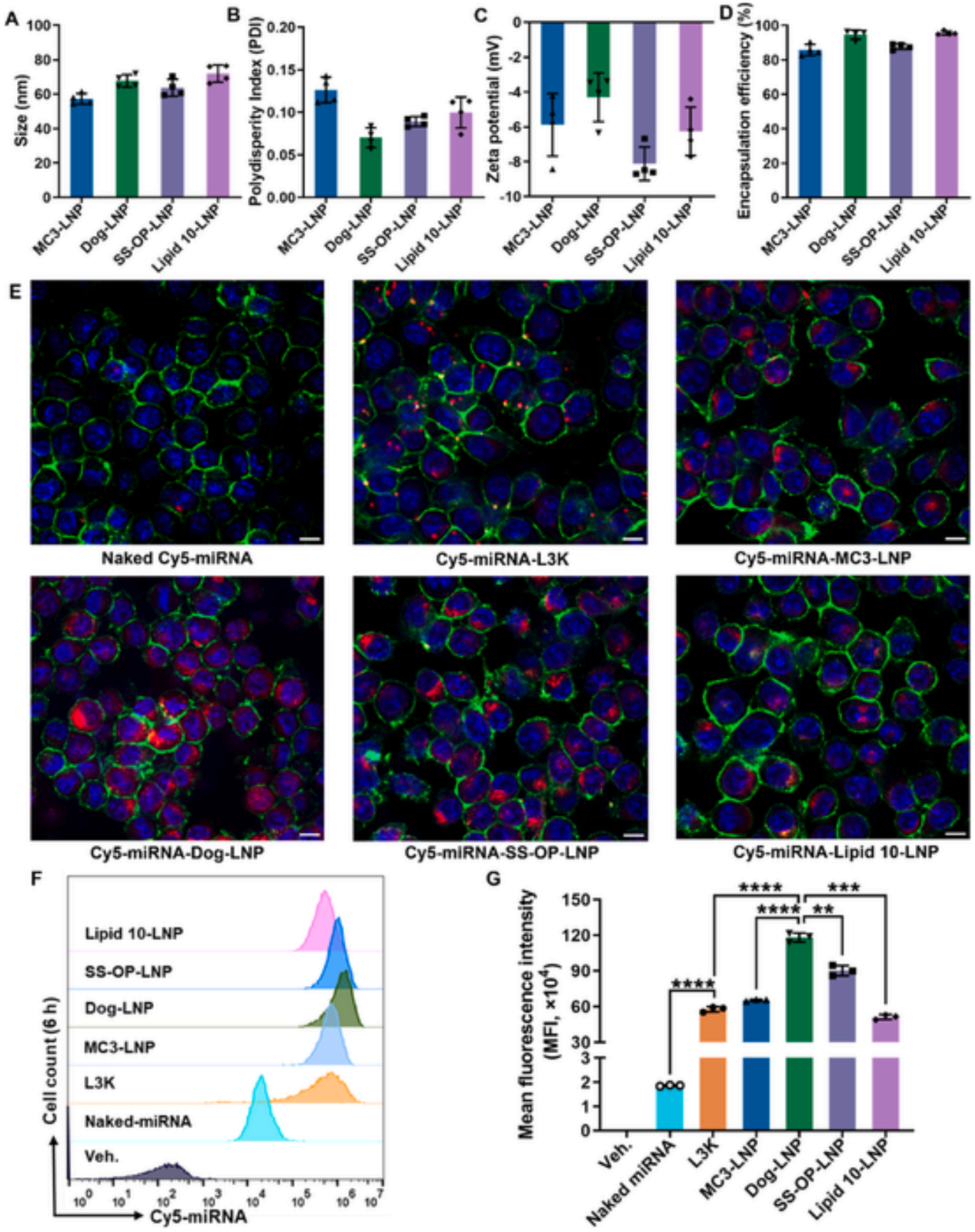
A
Size (nm)
100
80
60
40
20
0
MC3-LNP
Dog-LNP
SS-OP-LNP
Lipid 10-LNP
B
Polydisperity Index (PDI)
0.20
0.15
0.10
0.05
0.00
C
Zeta potential (mV)
0
-2
-4
-6
-8
-10
D
Encapsulation efficiency (%)
E
Naked Cy5-miRNA
Cy5-miRNA-L3K
Cy5-miRNA-MC3-LNP
Cy5-miRNA-Dog-LNP
Cy5-miRNA-SS-OP-LNP
Cy5-miRNA-Lipid 10-LNP
F
Lipid 10-LNP
SS-OP-LNP
Dog-LNP
MC3-LNP
L3K
Naked-miRNA
Veh.
Cell count (6 h)
Cy5-miRNA
G
Mean fluorescence intensity (MFI, ×10⁴)
150
120
90
60
30
3
2
1
0
****
***
**
Veh.
Naked miRNA
L3K
MC3-LNP
Dog-LNP
SS-OP-LNP
Lipid 10-LNP

Fig. 5. Cellular uptake of Cy5-miRNA-LNP by BV2 cells **A-D.** Characterization of physicochemical properties of each LNP formulation, including size, PDI, zeta potential, and EE (N = 4). **E.** Representative confocal laser scanning microscopy images of intracellular distribution of naked Cy5-miRNA, Cy5-miRNA-L3K, and Cy5-miRNA-LNP in BV2 cells 6 h after incubation. Cells were counterstained with DAPI (nuclei, blue) and WGA-AF488 (cell membrane, green). Scale bar, 10 μm. **F-G.** Quantification of miRNA cellular uptake after 6h of incubation of Cy5-labeled miRNA-L3K and miRNA-LNP in BV2 cells by flow cytometry. Data are presented as mean ± SD (N = 3, n = 3); $^{**}P < 0.01$, $^{***}P < 0.001$, $^{****}P < 0.0001$. (For interpretation of the references to colour in this figure legend, the reader is referred to the Web version of this article.)

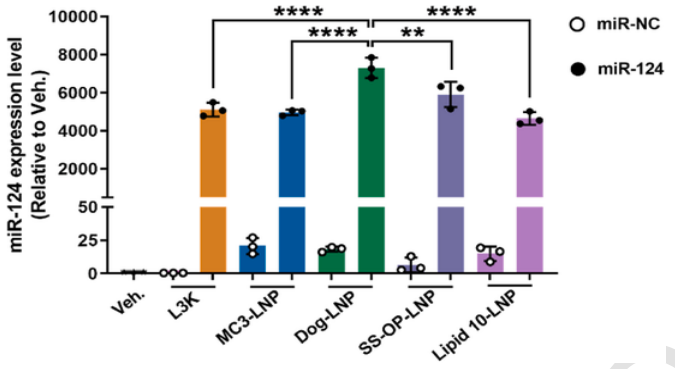

Fig. 6. *In vitro* transfection efficacy of miRNA-LNP in BV2 cells The *in vitro* transfection efficiency of miR-124 was determined by RT-qPCR in BV2 cells 24 h after treatment with 40 nM miR-NC or miR-124 mimic using L3K or LNP (N = 3, n = 3). Data are presented as mean ± SD; $^{**}P < 0.01$, $^{****}P < 0.0001$.

3.8. S–Ac7-DOG-LNP exhibit enhanced intramuscular miR-124 transfection and lower activation compared to MC3-LNP

Since S–Ac7-DOG-LNPs have never been used to deliver miRNA, nor in a context outside of vaccination, the aim here was to validate the efficacy of our formulation in a model in which S–Ac7-DOG-LNP were shown to be efficient [24]. MiR-124 loaded in S–Ac7-DOG-LNP were injected intramuscularly in the quadriceps femoris of mice (5 μg miRNA dose/mouse), and after 24 h, miR-124 and cytokine (IL-1β, IL-6 and MCP-1) expression levels were assessed (Fig. 10A). As positive control, we also loaded miR-124 in MC3-containing LNP. S–Ac7-DOG-LNP enabled higher miR-124 level at the site of injection than MC3-LNP and untreated mice (Fig. 10B). MiR-S-Ac7-DOG-LNP induced a slight decrease of PDE4B expression compared to miR-MC3-LNP (Fig. 10C), while the TRAF6 expression was significantly decreased after S–Ac7-DOG-LNP treatment compared to control and miR-MC3-LNP (Fig. 10D). Additionally, MC3-LNP induced an increase in IL-1β, IL-6 and MCP-1 mRNA levels compared to S–Ac7-DOG-LNP and untreated groups (Fig. 10E–G).

3.9. Injection of miR-124-S-Ac7-DOG-LNP in the brain reduced neuroinflammation in mice

LPS-induced systemic inflammation has been widely used as a neuroinflammatory model in rodents because of its ability to disrupt the BBB and trigger the subsequent migration of inflammatory cells and mediators from the circulation to the brain, leading to substantial exacerbation of neuroinflammation [40]. LPS-induced inflammation in mice was thus used to investigate the potential of miR-124-S-Ac7-DOG-LNP to reduce neuroinflammation. After intraperitoneal (i.p.) injection of LPS or saline, the mice received a local injection of miR-S-Ac7-DOG-LNP or miR-MC3-LNP into the prefrontal cortex (Fig. S9A). Compared to mice injected with saline, the mRNA levels of TNF-α, IL-6, and iNOS were increased in LPS-treated mice. Only the injection of S–Ac7-DOG-LNP in LPS-treated mice resulted in a higher miR-124 level (Fig. S9B). PDE4B expression was not affected regardless of the condition (Fig. S9C), while the TRAF6 expression was decreased after S–Ac7-DOG-LNP treatment (Fig. S9D). The LPS-induced increase of pro-inflammatory markers was significantly reduced by miR-124-S-Ac7-DOG-LNP, but not by miR-124-MC3-LNP (Fig. S9E–G). Based on these results we further explored the effects of miR-124-S-Ac7-DOG-LNP.

As described above, after i.p injection of LPS, mice received a local intracerebral injection of miR-124-LNP or miR–NC–LNP (Fig. 11A). The level of miR-124 was increased by a 5.8-fold by miR-124-LNP compared to miR–NC–LNP (Fig. 11B). When compared to the vehicle-treated LPS group, the administration of miR-124-LNP decreased the expression of TRAF6 (but not of PDE4B (Fig. 11C–D). LPS stimulation strongly enhanced the expression of TNF-α, IL-6, MCP-1, and iNOS in the prefrontal cortex, which was reversed by the administration of miR-124-LNP (Fig. 11E–H). Furthermore, miR-124-LNP also increased the gene expression of IL-10 ($p = 0.0591$) and CD206 compared to the controls (Fig. 11I–J), as well as miR-124-LNP increased the ratio of CD206/iNOS (M2/M1 markers) compared to the LPS group (Fig. S10).

3.10. Intravenous administration of miR-124-S-Ac7-DOG-LNP reduced neuroinflammation in mice

To further strengthen the therapeutic potential of the miR-124-S-Ac7-DOG-LNP, the LNP were administered by intravenous injection and their impact on neuroinflammation was evaluated as described above. After i.p injection of LPS, mice received 2 intravenous administration of miR-124-LNP or miR–NC–LNP (Fig. 12A). The level of miR-124 was increased by 1.8-fold compared to miR–NC–LNP (Fig. 12B). When compared to the vehicle-treated and miR–NC–treated LPS groups, the administration of miR-124-LNP decreased the expression of TRAF6 (Fig. 12C). LPS stimulation strongly enhanced the expression of TNF-α, IL-6, MCP-1, and iNOS in the prefrontal cortex, while the expression of TNF-α, IL-6 and iNOS was significantly decreased by the administration of miR-124-LNP (Fig. 12D–G). Furthermore, miR-124-LNP also significantly increased the gene expression of IL-10 and CD206 compared to the controls (Fig. 12H–I), as well as miR-124-LNP increased the ratio of CD206/iNOS (M2/M1 markers) compared to the LPS group (Fig. S11).

4. Discussion

Neuroinflammation, which results from intricate immune responses within the CNS, is a focal point of research in neurodegenerative diseases. Most neurodegenerative diseases lack reasonably effective therapies owing to the complexity of CNS functioning and the difficulty of therapeutics crossing the BBB. It has been suggested that miR-124 expression contributes to the suppression of neuroinflammation and, therefore, could be a promising therapeutic strategy for CNS pathologies [41]. However, the potential of miR-based therapeutics in the CNS is currently limited by the lack of safe and effective delivery systems. In recent years, LNP have rapidly emerged as efficient vehicles for RNA delivery; however, very few formulations have been specifically developed to deliver miRNA to the CNS. LNP are composed of different lipids, among which, an ionizable cationic lipid that is designed to encapsulate and release RNA cargo into the cytoplasm. This lipid has a strong impact on the behavior and performance of LNP. In the scope of neuroinflammation, the ionizable lipid must deliver the miRNA cargo into the cytoplasm but must not induce inflammation, as it might be desirable in the scope of vaccination. Here, we propose an LNP formulation able to deliver miRNA to the CNS, to modulate the inflammation toward a higher M2/M1-like ratio, without eliciting more inflammation. As far as we know, we provide, for the first time, a rational screening of clinically relevant LNP ionizable lipids for miRNA delivery, the

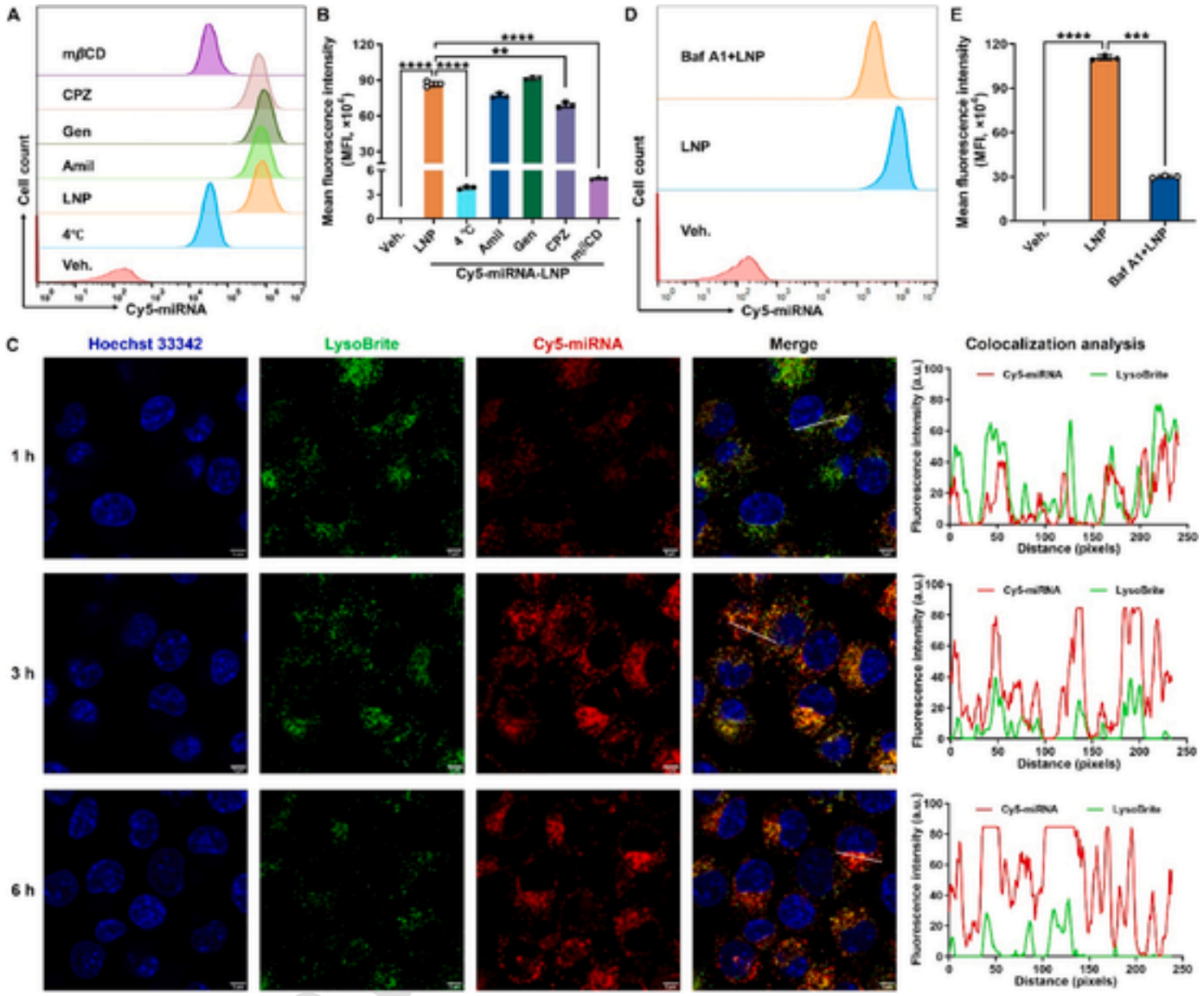

Fig. 7. Mechanism of S–Ac7-DOG-LNP-mediated miRNA uptake **A-B.** Representative flow cytometry analysis and the MFI analysis of BV2 cells incubated with different cell uptake inhibitors 1 h before co-incubation with Cy5-miR-124-LNP for 6 h. **C.** Representative confocal intracellular colocalization images of BV2 cells after Cy5-miR-124-LNP (Red) co-incubation for different time points. The acidic compartments were stained with LysoBrite™ (Green), and the nucleus was stained with Hoechst 33342 (Blue), respectively. Scale bar, 5 μm. **D-E.** Uptake of Cy5-miR-124-LNP by BV2 cells with or without Baf A1 addition using flow cytometry. Scale bar, 20 μm. Data are presented as mean ± SD (N = 3, n = 3); $^{**}P < 0.01$, $^{***}P < 0.001$, $^{****}P < 0.0001$. (For interpretation of the references to colour in this figure legend, the reader is referred to the Web version of this article.)

demonstration of the therapeutic efficacy of miR-124-S-Ac7-DOG LNP in an LPS-induced neuroinflammation model, and finally, a non-viral, clinically translatable delivery system for miRNA therapy in the CNS.

MiRNA are an endogenous non-coding small RNA that regulate gene expression by interacting with the 3′ untranslated region of the target mRNA to destabilize or repress mRNA translation [7,42]. MiRNA-124 has -5p and -3p mature miRNA types that can have different activities. While both miR-124-5p and -3p inhibited pro-inflammatory cytokine gene expression in LPS-activated BV2 cells, we showed for the first time that only miR-124-3p increased anti-inflammatory cytokine expression, suggesting that miR-124-3p could support the switch from a pro-inflammatory M1-like phenotype to an anti-inflammatory M2-like phenotype in activated microglial cells. This was consistent with previous studies that showed that miR-124-3p ameliorated intracerebral hemorrhage-induced inflammatory injury in mice potentially by modulating microglial polarization toward the M2 phenotype [9]. Similarly, Ponomarev et al. showed that miR-124-3p not only deactivates macrophages but also skews their polarization from an M1-like toward an M2-like phenotype [43]. Here, we showed that miR-124-3p reduces the expression of PDE4B and TRAF6 in BV2 cells and primary MGCs. However, we cannot completely assert that miR-124-3p acts on inflammation directly via PDE4B and TRAF6, even if they are important regulators of inflammation. PDE4B, a member of the type IV cAMP-specific cyclic nucleotide PDE family, regulates the cellular concentration of cyclic nucleotides and thus plays a role in the signal transduction of inflammatory factors [44]. PDE4B knockdown effectively inhibits LPS-induced nuclear factor kappa-B (NF-κB) activation and inflammatory responses [45]. TRAF6 is a crucial signal transducer that mediates activation of the NF-κB pathway after Toll-like receptor 4 (TLR4) activation [46]. Additionally, TRAF6 also mediates downstream activation of p38 MAPK and c-jun N-terminal kinase (JNK) pathways, which all contribute to the macrophage polarization toward a M1-like phenotype

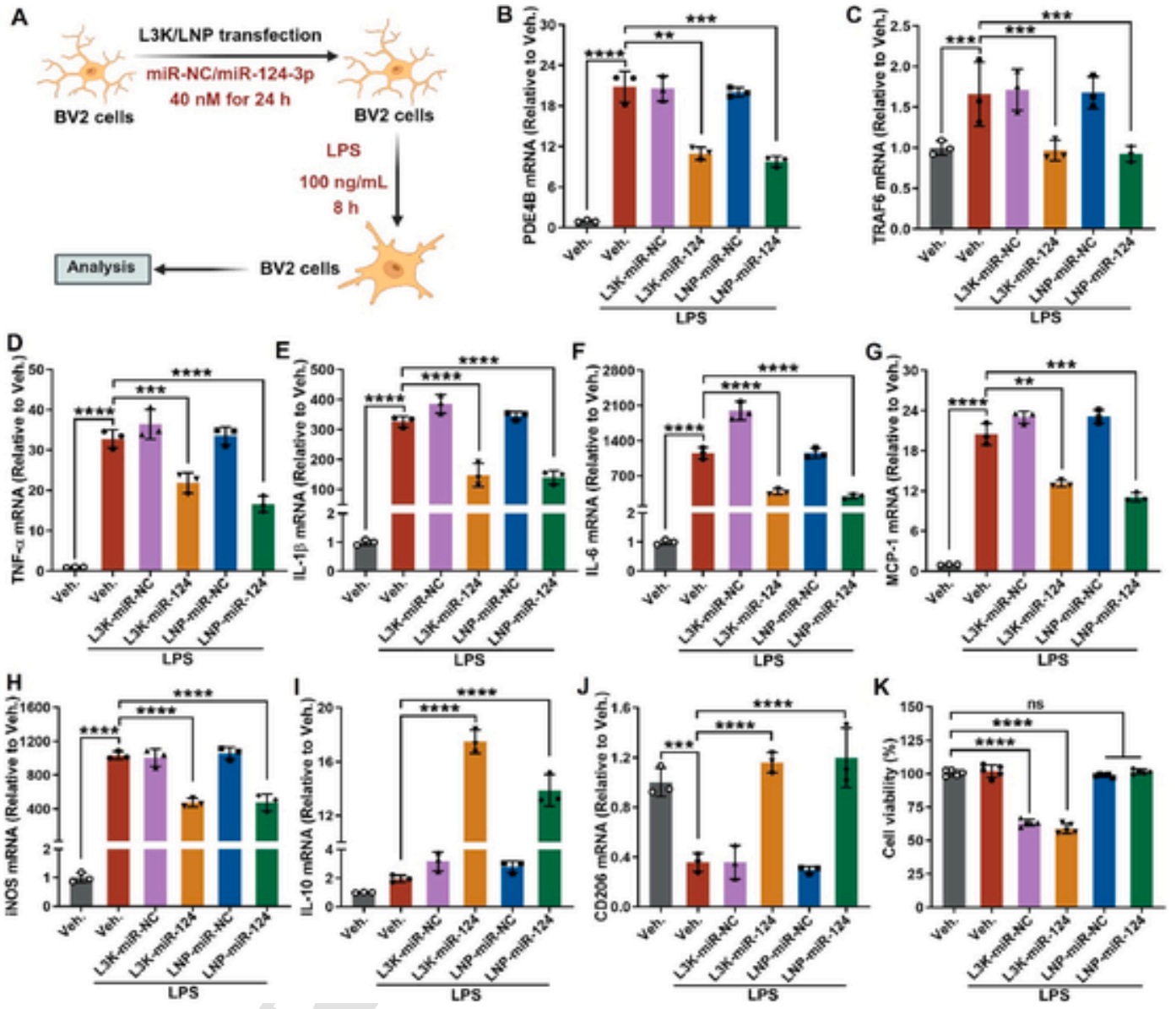

Fig. 8. Impact of miR-124-Dog-LNP on inflammation markers in LPS-activated BV2 cells **A.** Schematic illustration of experimental settings. Cells were transfected with miR-NC or miR-124-3p mimics using L3K or LNP for 24 h, followed by stimulation with LPS for 8 h. **B-J**. RT-qPCR analysis of PDE4B (B), TRAF6 (C), TNF-α (D), IL-1β (E), IL-6 (F), MCP-1 (G), iNOS (H), IL-10 (I), and CD206 (J) levels in BV2 cells, pretreated with miR-NC or miR-124-3p-LNP for 24 h followed by 8 h LPS (100 ng/mL) (N = 3, n = 3). **K**. The cytotoxicity of miR–NC–L3K, miR-124-L3K, miR–NC–LNP, and miR-124-LNP was tested in BV2 cells using the MTT assay (N = 4, n = 5). Data are presented as mean ± SD; $^{**}P < 0.01$, $^{***}P < 0.001$, $^{****}P < 0.0001$, ns, not significant, $P > 0.05$.

[47]. Literature and our data support that miR-124-3p is a promising candidate for the treatment of neuroinflammatory diseases.

The successful outcomes of LNP-based nucleic acid therapies in numerous preclinical and clinical studies are attributed to important LNP characteristics such as optimal size and zeta potential range, excellent stability in biological fluids, superior biocompatibility, and high effectiveness in the cellular transfection process [15]. In recent years, most developments in the context of LNP formulations have focused on mRNA/siRNA-based therapies, while few publications have reported miRNA-loaded LNP formulations. Notably, previous studies reporting the use of LNP to deliver miRNA to the brain have been limited to cancer therapy [48]. The development of LNP for delivering miRNA in the context of neuroinflammation represents thus a significant gap in the field of neuro-nanomedicine. In this study, we used the lipid molar ratio classically reported in the literature and used for the Onpattro® siRNA drug product and we tested different N:P ratio and lipid concentrations. The best compromise between LNP size, miRNA encapsulation efficiency and stability was obtained when using 8 mM of lipids and a N:P ratio of 10:1. We observed that the zeta potential of LNPs with a higher N:P ratio (10:1) was more stable over 28 days at 4 °C compared to those with a lower N:P ratio (6:1). We hypothesize that this stability reflects better electrostatic shielding and structural integrity of the particles, likely due to a higher density of ionizable lipids complexing the RNA payload. In contrast, lower N:P formulations may contain a larger proportion of uncomplexed RNA and/or free lipids, which could rearrange over time or interact with the storage medium, thereby causing fluctuations in surface charge [49]. As a helper lipid, DOPE is known to promote non-bilayer (hexagonal) phase structures, which enhance endosomal escape but can compromise bilayer rigidity and thus affect physical stability during storage [37]. In contrast, DSPC favors more rigid bi-

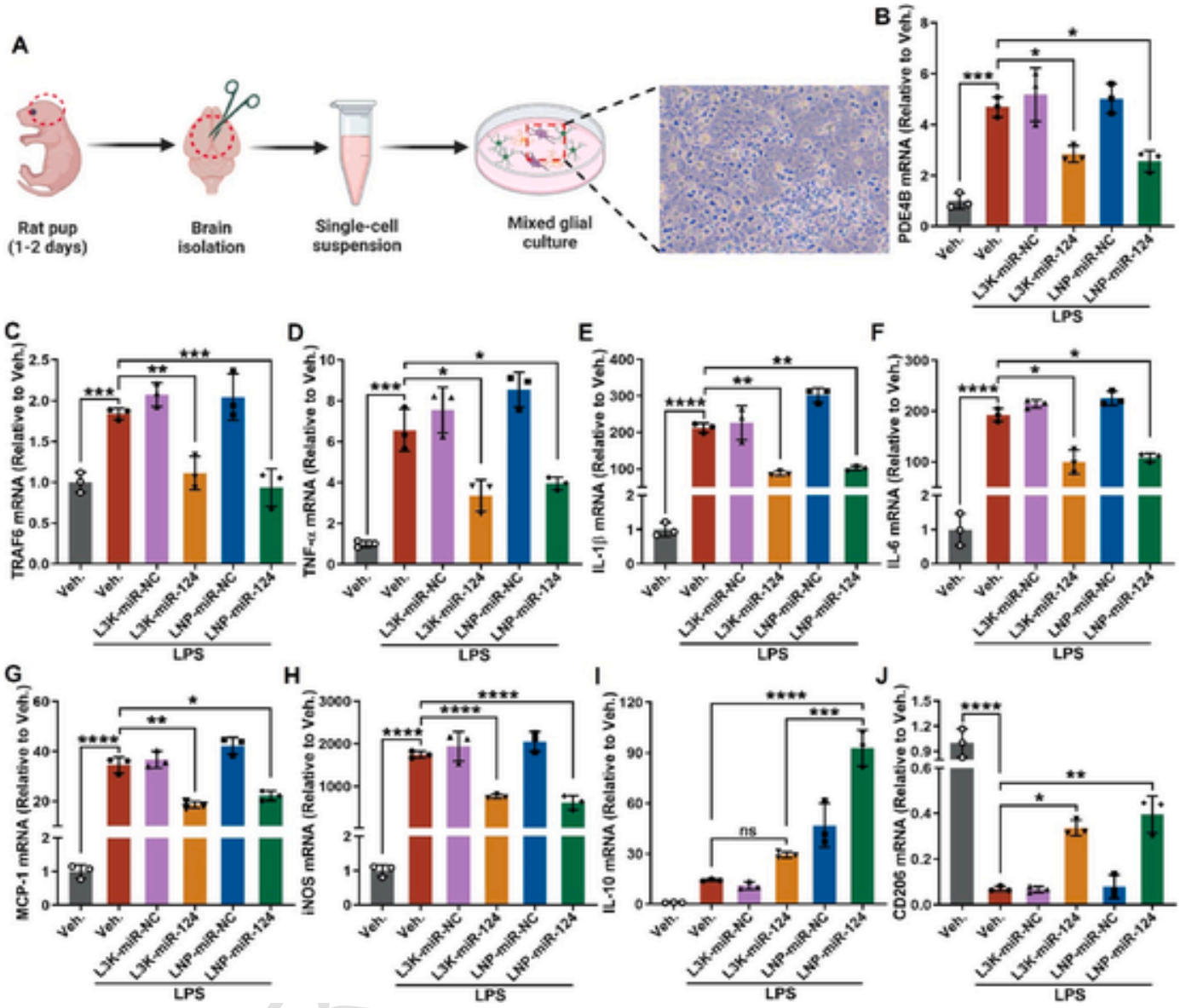

Fig. 9. Impact of miR-124-Dog-LNP on inflammation markers in LPS-activated MGC **A.** Experimental setting for the isolation of primary MGC. **B-J**. Gene expression analysis of PDE4B (B), TRAF6 (C), TNF-α (D), IL-1β (E), IL-6 (F), MCP-1 (G), iNOS (H), IL-10 (I), and CD206 (J) in MGC pretreated with miR-NC or miR-124-LNP for 24 h followed by 8 h of LPS (100 ng/mL) (N = 3, n = 3). Data are presented as mean ± SD; *$P < 0.05$, **$P < 0.01$, ***$P < 0.001$, ****$P < 0.0001$, ns, not significant, $P > 0.05$.

layer structures and is often associated with improved long-term stability. In our study, we prioritized DOPE to support intracellular delivery efficiency and accept a potential trade-off in physical stability. Nonetheless, the high N:P ratio formulations remained stable over 28 days, which suggests that the ionizable lipid content compensated for the use of DOPE.

Ionizable lipids are a vital component of LNP, enabling efficient RNA association and delivery to the cytoplasm while exhibiting significantly lower cytotoxicity than cationic lipids [50,51]. Several ionizable lipids with different properties and efficiencies are now available, but their therapeutic efficiency depends strongly on the desired effect and the cells the LNP are designed for. As not much is reported in the literature, we determined which ionizable lipid would be the most efficient for delivering miR-124 to microglial cells and modulating inflammation, comparing six different ionizable lipids (*i.e.*, MC3, SM102, C12-200, Dog, SS-OP, and Lipid 10) to formulate LNP. These lipids were selected based on information reported in the literature and their relevance to our application. To make this screening more time-efficient, we used Luc-siRNA loaded LNP and tested their impact on the activation and Luc silencing of BV2 cells expressing Luc. The physicochemical properties of siRNA and miRNA mimics could be considered similar (double strand, approximately 21 nucleotides), to the contrary to the much larger mRNA molecules [52]. While the 6 LNP had the same physico-chemical characteristics, C12-200-LNP was the only one inducing the activation of resting BV2 cells, and with SM-102-LNP, were toxic at the highest concentrations (40–80 nM). Interestingly, Meulewaeter et al. observed a marked increase in IL-6 and MCP-1 levels in animals that received C12-200 LNP via intramuscular injection [53]. In contrast, SM-102 LNP were significantly less potent in inducing IL-6 expression, resulting in cytokine levels approximately 10 times lower than with C12-200 LNP [53]. While such immune activation could be a desirable advantage for vaccination, in other indications, it can be

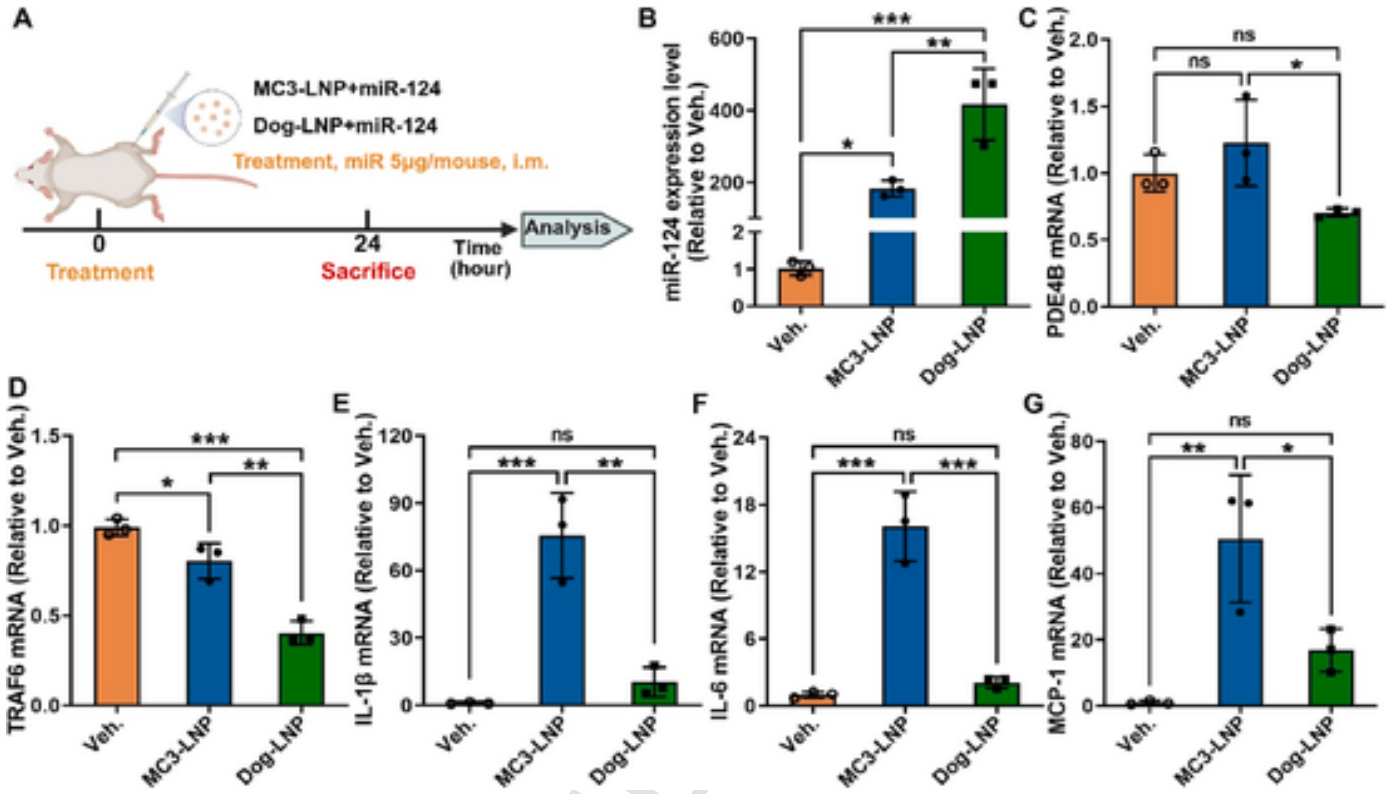

Fig. 10. Impact of miR-124-Dog-LNP on intramuscular gene expression **A**. Swiss mice were injected with miR-MC3-LNP and miR-S-Ac7-DOG-LNP at a 5 μg of miR-124 in the quadricep of the lower right leg. **B**. *In vivo* transfection efficiency of miR-124 was determined by RT-qPCR in quadricep at 24 h after treatment (n = 3). **C-G**. The mRNA expression levels of PDE4B, TRAF6, and cytokines (IL-1β, IL-6 and MCP-1) in tissues were determined by RT-qPCR in quadricep at 24 h after treatment (n = 3). Data are presented as mean ± SD; $^{*}P < 0.05$, $^{**}P < 0.01$, $^{***}P < 0.001$, ns, not significant, $P > 0.05$.

detrimental to the treatment success and predispose patients to unexpected adverse reactions [54]. S–Ac7-DOG is a biodegradable ionizable lipid composed of a reducible disulfide bond, a cyclic ionizable amine head group, and dioleoyl tails connected via ester linkages [55]. Upon cellular uptake and exposure to the intracellular reducing environment, both the disulfide and ester bonds are cleaved, promoting rapid LNP disintegration and RNA [56]. This limits lipid accumulation in tissues, which is a known contributor to reduced inflammation at the injection site and enhanced tolerability [57,58]. Recent findings suggest that rapidly biodegradable ionizable lipids, such as S–Ac7-DOG, generate small, reparable pores in endosomal membranes that trigger the recruitment of the ESCRT complex, thereby avoiding sustained endosomal damage [59]. This contrasts with non-degradable ionizable lipids, which may induce irreversible membrane damage, leading to heightened immune activation [59]. Thus, S–Ac7-DOG allows for efficient RNA release with minimal activation of danger signals. Finally, the dioleoyl tails of S–Ac7-DOG promote LNP membrane fluidity and non-lamellar phase formation, which may enhance fusion with endosomal membranes and reduce mechanical disruption of cellular membranes, a known trigger of inflammation [60]. This could also contribute to the milder immune activation observed.

Regarding Luc knockdown, the highest efficiency was obtained for the SS-OP-LNP and S–Ac7-DOG-LNP. Both lipids have a disulfide bond that can be cleaved in the reductive environment of the cytoplasm [61,62]. This is thought to trigger the dissociation of the particles and a fast release of miRNA in the cytoplasm, which mediates rapid gene silencing [61,62]. Ionizable lipid structure-function relationship with endosomal escape can be found in an excellent in-depth review [51]. The ionizable lipid is not the only ingredient impacting the LNP formulation and efficiency. This is the reason why, contrary to the reference formulations (namely Onpattro® and Moderna®), we selected DOPE and DSPE-PEG as the helper and PEGylated lipids. DSPE-PEG provides higher stability to the LNP. However, high stability might limit cell interactions and thus lead to low cellular uptake, poor endosomal escape and reduced efficiency of the mRNA-based therapeutics. This is known as the PEG dilemma [63]. So, we opted to compensate the potential impact of an increased stability brought by the DSPE-PEG on therapeutic efficiency with DOPE, which would favor a higher endosomal escape by high membrane fusion capacity [64].

We then focused on SS-OP, S–Ac7-DOG, Lipid 10, and MC3-LNP for the next steps aiming to encapsulate miR-124 and study cell uptake. No impact of the cargo (miRNA vs siRNA) on LNP physico-chemical properties was observed, while S–Ac7-DOG-LNP had the highest miR-124 transfection efficiency. This correlated with the highest cellular uptake of S–Ac7-DOG-LNP. S–Ac7-DOG was recently developed by the De Geest's lab as a reduction-sensitive ionizable cationic lipid that, when formulated with mRNA in LNP, induces relatively low reactogenicity upon intramuscular injection in mice [24]. S–Ac7-DOG-LNP can escape from the endosomes where the disulfide and ester bonds are degraded, leading to the disintegration of the whole LNP and accelerating the release of RNA, thus improving their efficiency [51]. Additionally, the unsaturated oleic acid alkyl tails of S–Ac7-DOG increase LNP membrane fluidity and tend to form a non-bilayer phase, which further facilitates endosomal membrane disruption and cargo release [60]. SS-OP also has ester and disulfide bonds, and two unsaturated hydrophobic tails. However, the position and steric effect of the ester groups can greatly affect ionizable lipid clearance and potency [65]. Furthermore, we observed that the internalization of S–Ac7-DOG-LNP was strictly energy-dependent, involved V-ATPase-dependent pathways, and cholesterol appeared to be required for S–Ac7-DOG-LNP internalization. However,

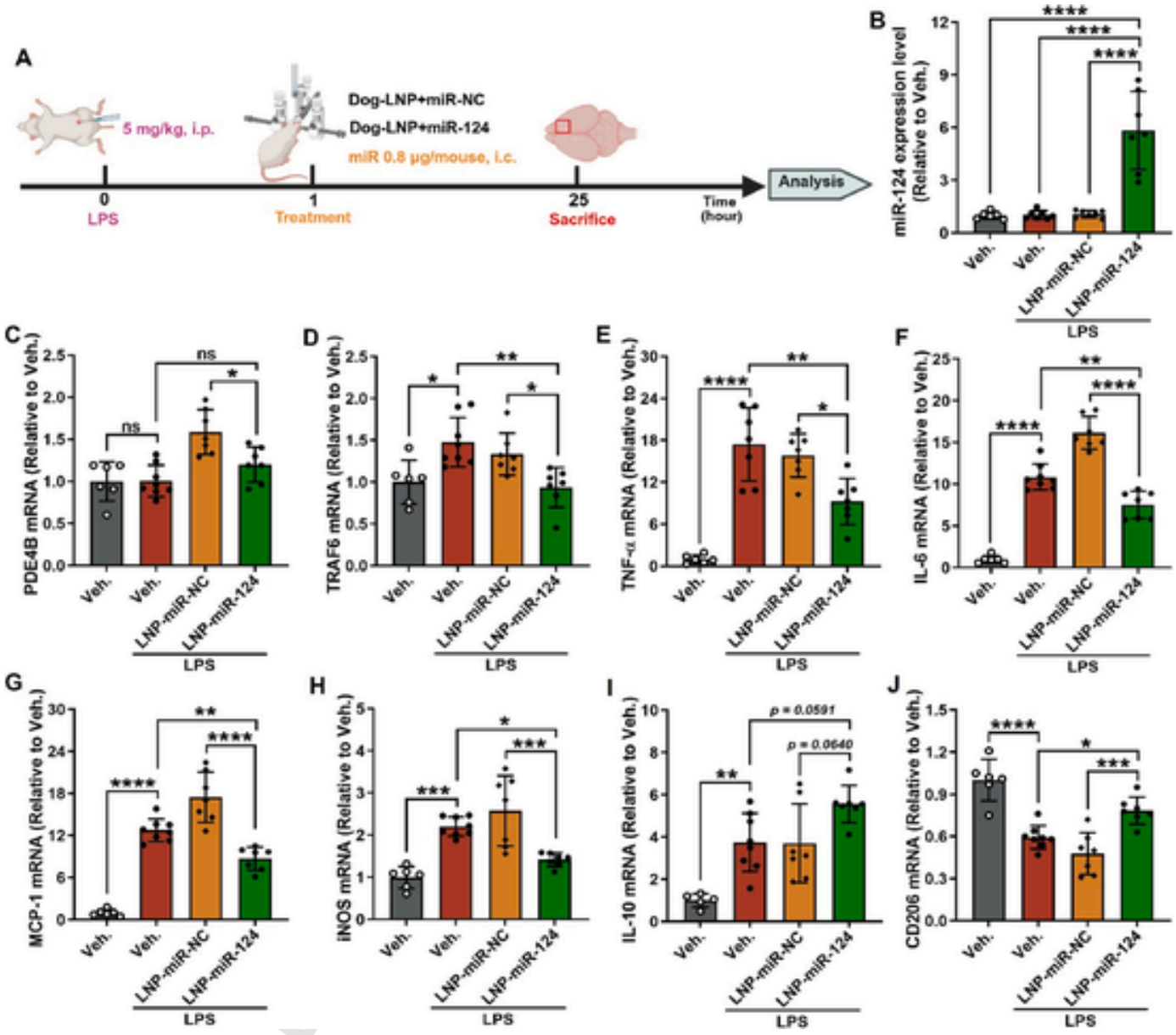

Fig. 11. Impact of miR-124-S-Ac7-DOG-LNP on LPS-induced neuroinflammation after brain injection **A.** Experimental setting: LPS was injected at 5 mg/kg i.p., and 1 h later was followed by intracerebral (i.c.) injection of LNP containing either miR-NC or miR-124. One day later, the mice were sacrificed, and the prefrontal cortex was collected to analyze gene expression. **B.** The levels of miR-124 after LNP treatment for 24 h. **C-J**. Relative mRNA levels of PDE4B (C), TRAF6 (D), TNF-α (E), IL-6 (F), MCP-1 (G), iNOS (H), IL-10 (I), and CD206 (J). Data are presented as mean ± SD (n = 6–8); $^{*}P < 0.05$, $^{**}P < 0.01$, $^{***}P < 0.001$, $^{****}P < 0.0001$, ns, not significant, $P > 0.05$.

further experiments are needed to determine if lipid raft disruption and clathrin-mediated endocytosis are involved. Confocal laser scanning microscopy images showed increased amounts of miRNA escaping from the endosomes and diffusing into the cytoplasm over time. Combined with a decrease of the endosomal staining, which could be attributed to the destruction of the lysosomal compartments resulting from the proton sponge effect of the LNP [66], we can assume that S–Ac7-DOG-LNP could successfully escape the endosomes and deliver miRNA to the cytoplasm. Thus, S–Ac7-DOG-LNP was selected for the functional evaluation of miR-124-LNP.

Microglia are generally considered as the resident macrophages in the CNS and act as critical regulators of neuroinflammation, whose activated phenotype can go along a wide spectrum from "classically activated" pro-inflammatory (M1-like) to "alternatively activated" anti-inflammatory (M2-like) in response to different stimuli [67]. The miR-124-LNP reduced the gene expression of the main pro-inflammatory microglial markers and promoted their anti-inflammatory markers in LPS-induced BV2 cells. S–Ac7-DOG-LNP were not toxic, contrary to lipofectamine, one of the most used *in vitro* transfection reagents, which induced a 50 % cell death. This is consistent with previous reports [68,69]. Although commercial transfection reagents are useful as *in vitro* positive controls, their severe systemic toxicity makes them unsuitable for *in vivo* applications [51]. We further confirmed the results obtained in BV2 cells in primary mixed glial cells (MGCs), even if the more complex nature of cell interactions (astrocytes, microglia, oligodendrocytes) in the MGC model could induce some differences. Collectively, these findings support the use of S–Ac7-DOG-LNP-mediated miR-124 delivery as a potential therapeutic tool for neuroinflammatory diseases.

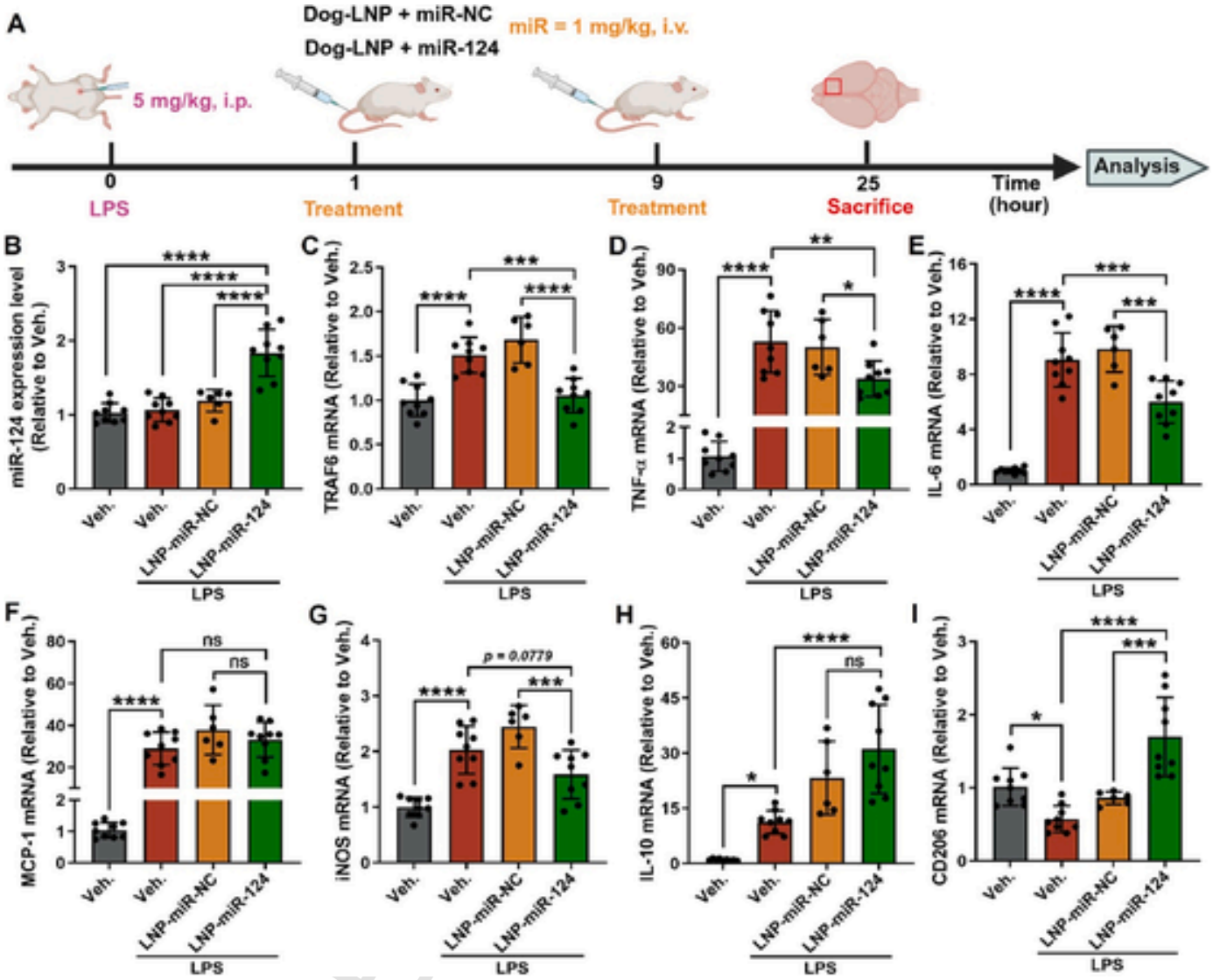

Fig. 12. Impact of miR-124-S-Ac7-DOG-LNP after systemic injection on LPS-induced neuroinflammation **A.** Experimental setting: LPS was injected at 5 mg/kg i.p., and 1 h and 9 h later was followed by intravenous (i.v.) injection of LNP containing either miR-NC or miR-124. One day later, the mice were sacrificed, and the prefrontal cortex was collected to analyze gene expression of inflammatory markers. **B.** The levels of miR-124 after LNP treatment for 24 h. **C–I**. Relative mRNA levels of TRAF6 (C), TNF-α (D), IL-6 (E), MCP-1 (F), iNOS (G), IL-10 (H), and CD206 (I). Data are presented as mean ± SD (n = 6–9); $^{*}P < 0.05$, $^{**}P < 0.01$, $^{***}P < 0.001$, $^{****}P < 0.0001$, ns, not significant, $P > 0.05$.

As S–Ac7-DOG-LNP were initially developed for vaccination by intramuscular injection and have never been used before to deliver miRNA, we first evaluated the efficiency of S–Ac7-DOG-LNP for transfection of miR-124 *in vivo* after intramuscular injection. MC3-LNP were used as a positive control, being one of the most used ionizable lipids for mRNA delivery. Both LNP were able to transfect miR-124, but miRNA levels in the muscle were higher with S–Ac7-DOG-LNP, and to the contrary of MC3-LNP, did not increase the expression of pro-inflammatory markers. This is consistent with another study comparing pro-inflammatory cytokine levels in the serum after intramuscular injection of MC3-LNP and S–Ac7-DOG-LNP in mice [24]. It was also reported that S–Ac7-DOG-LNP induced longer-lasting expression and higher expression levels of Luc mRNA in the injected muscle while showing less accumulation in the liver. Thus, S–Ac7-DOG-LNP may be less prone to the induction of undesired off-target effects. Moreover, other studies have reported that LNP can induce pro-inflammatory immune responses, which might be desirable for vaccination but much less so for neuroinflammation [70,71]. Chen et al. reviewed how each component of LNP could contribute to their overall immunogenicity as well as the potential immune responses involved [72]. LNP can activate TLR4 and NLRP3, which can then induce the secretion of IL-1β, IFN-γ, and IL-6 through the innate immunity pathway and can promote $CD8^{+}$ T cell and T Follicular helper cell responses. Recent research has shown that some amine headgroups in ionizable lipids drive LNP immunogenicity by binding to TLR4 and CD1d and promoting lipid raft formation [73]. Taken together, these data indicated that S–Ac7-DOG-LNP have higher transfection efficiency and less pro-inflammatory effects than MC3-LNP.

As a proof-of-concept, miR-124-S-Ac7-DOG-LNP were injected into the prefrontal cortex of LPS-treated mice. Indeed, intracerebral or intracerebroventricular local injections of LNP have been shown to successfully deliver mRNA into neurons and astrocytes [34,74,75]. We successfully delivered miR-124 into the brain by localized and systemic injections, resulting in inhibition of pro-inflammatory markers expression. It also promoted an increase of anti-inflammatory markers as observed *in vitro*, which confirmed that S–Ac7-DOG-LNP can efficiently

deliver miR-124 into the CNS and could be used as a therapy to modulate neuroinflammation.

5. Conclusion

We report here the development of an original LNP formulation able to deliver miRNA to the CNS, to modulate the inflammation toward a higher M2/M1-like ratio compared to LNP containing the "gold-standard" ionizable lipids, without eliciting more inflammation. As far as we know, we provide, for the first time, a rational screening of clinically relevant LNP ionizable lipids for miRNA delivery, the demonstration of the therapeutic efficacy of miR-124-S-Ac7-DOG LNP in an LPS-induced neuroinflammation model, and finally a non-viral, clinically translatable delivery system for miRNA therapy in the CNS. To design the next generation of non-invasive gene therapies, future studies should investigate the delivery of LNP via different routes and how targeting them could improve their efficiency while limiting off-target effects.

CRediT authorship contribution statement

Zhanjun Ma: Writing – original draft, Visualization, Methodology, Investigation, Formal analysis, Data curation. **Hong Anh Dang:** Writing – review & editing, Resources, Methodology, Investigation, Formal analysis. **Jingjing Yang:** Writing – review & editing, Resources, Methodology, Formal analysis. **Giulia Rodella:** Writing – review & editing, Methodology, Formal analysis. **Ariane Mwema:** Writing – review & editing, Validation, Methodology, Data curation. **Emily De Lombaerde:** Resources, Methodology. **Yong Chen:** Resources, Methodology. **Bruno G. De Geest:** Writing – review & editing, Resources, Methodology, Investigation. **Vincent van Pesch:** Writing – review & editing, Resources, Methodology, Investigation, Funding acquisition. **Giulio G. Muccioli:** Writing – review & editing, Supervision, Project administration, Investigation, Funding acquisition, Conceptualization. **Anne des Rieux:** Writing – review & editing, Supervision, Resources, Project administration, Investigation, Funding acquisition, Conceptualization.

Declaration of competing interest

The authors declare the following financial interests/personal relationships which may be considered as potential competing interests:Bruno De Geest and Yong Chen have patent #WO2022136641A1 licensed to etherna. If there are other authors, they declare that they have no known competing financial interests or personal relationships that could have appeared to influence the work reported in this paper.

Acknowledgments

Zhanjun Ma was supported by a China Scholarship Council (CSC) fellowship. Anne des Rieux, Giulio Muccioli and Vincent van Pesch are supported by Fonds de la Recherche Scientifique—Fonds National de la Recherche Scientifique (FRS-FNRS) (Belgium), the Action de Recherche Concertée (ARC) EViM and the Fondation Charcot Stichting. The authors thank Prof. Thomas Michiels (de Duve Institute, UCLouvain) for the generation of luciferase-BV2 cells, and Prof Donatienne Tyteca (de Duve Institute, UCLouvain), Dr. Paloma Lozano Picazo and Dr. Ana Santos Coquillat (LDRI, UCLouvain) for their help and advice with the uptake experiments. The authors would like to thank the Fondation Louvain for funding the acquisition of the Ignite instrument.

Data availability

Data will be made available on request.

Appendix A. Supplementary data

Supplementary data to this article can be found online at https://doi.org/10.1016/j.biomaterials.2025.123589.

References

[1] Y. Xu, et al., Ripks and neuroinflammation, Mol. Neurobiol. 61 (9) (2024) 6771–6787.
[2] Y. Pan, et al., Second Near-infrared macrophage-biomimetic nanoprobes for photoacoustic imaging of neuroinflammation, Mol. Pharm. 21 (4) (2024) 1804–1816.
[3] H. Wang, et al., Target modulation of glycolytic pathways as a new strategy for the treatment of neuroinflammatory diseases, Ageing Res. Rev. 101 (2024) 102472.
[4] S. Hickman, et al., Microglia in neurodegeneration, Nat. Neurosci. 21 (10) (2018) 1359–1369.
[5] R. Qasim, et al., The Nurr1 ligand indole acetic acid hydrazide loaded onto ZnFe2O4 nanoparticles suppresses proinflammatory gene expressions in SimA9 microglial cells, Sci. Rep. 14 (1) (2024) 13987.
[6] A.N. Galindo, D.A. Frey Rubio, M.H. Hettiaratchi, Biomaterial strategies for regulating the neuroinflammatory response, Mater. Adv. 5 (10) (2024) 4025–4054.
[7] F.C. Moraes, et al., miRNA delivery by Nanosystems: state of the art and perspectives, Pharmaceutics 13 (11) (2021).
[8] J. Zhao, Z. He, J. Wang, MicroRNA-124: a key player in microglia-mediated inflammation in neurological diseases, Front. Cell. Neurosci. 15 (2021) 771898.
[9] A. Yu, et al., MiR-124 contributes to M2 polarization of microglia and confers brain inflammatory protection via the C/EBP-α pathway in intracerebral hemorrhage, Immunol. Lett. (2017) 182.
[10] P. Periyasamy, et al., Cocaine-mediated downregulation of miR-124 activates microglia by targeting KLF4 and TLR4 signaling, Mol. Neurobiol. 55 (4) (2018) 3196–3210.
[11] Z. Xu, et al., MicroRNA-124 improves functional recovery and suppresses Bax-dependent apoptosis in rats following spinal cord injury, Mol. Med. Rep. 19 (4) (2019) 2551–2560.
[12] X. Du, et al., miR-124 downregulates BACE 1 and alters autophagy in APP/PS1 transgenic mice, Toxicol. Lett. 280 (2017) 195–205.
[13] K.A.O. Gandy, et al., Resveratrol (3, 5, 4'-Trihydroxy-trans-Stilbene) attenuates a mouse model of multiple sclerosis by altering the miR-124/sphingosine kinase 1 Axis in encephalitogenic T cells in the brain, J. Neuroimmune Pharmacol. 14 (3) (2019) 462–477.
[14] J. Zhang, et al., MicroRNA-125a-Loaded polymeric nanoparticles alleviate systemic lupus erythematosus by restoring effector/regulatory T cells balance, ACS Nano 14 (4) (2020) 4414–4429.
[15] P.R. Cullis, M.J. Hope, Lipid nanoparticle systems for enabling gene therapies, Mol. Ther. : the Journal of the American Society of Gene Therapy 25 (7) (2017) 1467–1475.
[16] X. Hou, et al., Lipid nanoparticles for mRNA delivery, Nat. Rev. Mater. 6 (12) (2021) 1078–1094.
[17] A. Akinc, et al., The Onpattro story and the clinical translation of nanomedicines containing nucleic acid-based drugs, Nat. Nanotechnol. 14 (12) (2019) 1084–1087.
[18] M. Li, et al., Secreted expression of mRNA-encoded truncated ACE2 variants for SARS-CoV-2 via lipid-like nanoassemblies, Adv. Mater. (Deerfield Beach, Fla.) 33 (34) (2021) e2101707.
[19] Y. Eygeris, et al., Chemistry of lipid nanoparticles for RNA delivery, Accounts Chem. Res. 55 (1) (2022).
[20] X. Han, et al., An ionizable lipid toolbox for RNA delivery, Nat. Commun. 12 (1) (2021) 7233.
[21] F. Ma, et al., Neurotransmitter-derived lipidoids (NT-lipidoids) for enhanced brain delivery through intravenous injection, Sci. Adv. 6 (30) (2020) eabb4429.
[22] V. Passos Gibson, et al., Hyaluronan decorated layer-by-layer assembled lipid nanoparticles for miR-181a delivery in glioblastoma treatment, Biomaterials 302 (2023) 122341.
[23] A. Badr, et al., Microglia-targeted inhibition of miR-17 via mannose-coated lipid nanoparticles improves pathology and behavior in a mouse model of Alzheimer's disease, Brain Behav. Immun. 119 (2024) 919–944.
[24] E. De Lombaerde, et al., Combinatorial screening of biscarbamate ionizable lipids identifies a low reactogenicity lipid for lipid nanoparticle mRNA delivery, Adv. Funct. Mater. 34 (21) (2024) 2310623.
[25] B. Lizcano-Perret, et al., Cardiovirus leader proteins retarget RSK kinases toward alternative substrates to perturb nucleocytoplasmic traffic, PLoS Pathog. 18 (12) (2022) e1011042.
[26] V.E. Miron, et al., M2 microglia and macrophages drive oligodendrocyte differentiation during CNS remyelination, Nat. Neurosci. 16 (9) (2013) 1211–1218.
[27] Y. Labrak, et al., The combined administration of LNC-encapsulated retinoic acid and calcitriol stimulates oligodendrocyte progenitor cell differentiation in vitro and in vivo after intranasal administration, Int. J. Pharm. 659 (2024) 124237.
[28] R. Ray, et al., Direct membrane penetration and cytosolic delivery of nanoparticles via electrostatically bound amphiphiles, ACS Appl. Mater. Interfaces 16 (13) (2024) 15819–15831.
[29] Y. Liu, et al., Imidazolyl lipids enhanced LNP endosomal escape for ferroptosis RNAi treatment of cancer, Small 20 (40) (2024) e2402362.
[30] V. Mutemberezi, et al., Oxysterol levels and metabolism in the course of neuroinflammation: insights from in vitro and in vivo models, J. Neuroinflammation 15 (1) (2018) 74.

[31] L. Qin, et al., Systemic LPS causes chronic neuroinflammation and progressive neurodegeneration, Glia 55 (5) (2007) 453–462.
[32] R. Gordon, et al., Protein kinase Cδ upregulation in microglia drives neuroinflammatory responses and dopaminergic neurodegeneration in experimental models of Parkinson's disease, Neurobiol. Dis. 93 (2016).
[33] L.E. Waggoner, K.F. Miyasaki, E.J. Kwon, Analysis of PEG-lipid anchor length on lipid nanoparticle pharmacokinetics and activity in a mouse model of traumatic brain injury, Biomater. Sci. 11 (12) (2023) 4238–4253.
[34] M.C. Palumbo, et al., MicroRNA137-loaded lipid nanoparticles regulate synaptic proteins in the prefrontal cortex, Mol. Ther. 31 (10) (2023) 2975–2990.
[35] S. Gimondi, et al., Microfluidic devices: a tool for nanoparticle synthesis and performance evaluation, ACS Nano 17 (15) (2023) 14205–14228.
[36] S. Xu, et al., Tumor-tailored ionizable lipid nanoparticles facilitate IL-12 circular RNA delivery for enhanced lung cancer immunotherapy, Adv. Mater. (Deerfield Beach, Fla.) 36 (29) (2024) e2400307.
[37] C. Hald Albertsen, et al., The role of lipid components in lipid nanoparticles for vaccines and gene therapy, Adv. Drug Deliv. Rev. 188 (2022) 114416.
[38] J. Karlsson, et al., Photocrosslinked bioreducible polymeric nanoparticles for enhanced systemic siRNA delivery as cancer therapy, Adv. Funct. Mater. 31 (17) (2021).
[39] B. Hu, et al., Thermostable ionizable lipid-like nanoparticle (iLAND) for RNAi treatment of hyperlipidemia, Sci. Adv. 8 (7) (2022) eabm1418.
[40] A. Skrzypczak-Wiercioch, K. Sałat, Lipopolysaccharide-induced model of neuroinflammation: mechanisms of action, research application and future directions for its use, Molecules 27 (17) (2022).
[41] J. Xu, et al., miR-124: a promising therapeutic target for central nervous system injuries and diseases, Cell. Mol. Neurobiol. 42 (7) (2022) 2031–2053.
[42] M.R. Friedländer, et al., Discovering microRNAs from deep sequencing data using miRDeep, Nat. Biotechnol. 26 (4) (2008) 407–415.
[43] E.D. Ponomarev, et al., MicroRNA-124 promotes microglia quiescence and suppresses EAE by deactivating macrophages via the C/EBP-α-PU.1 pathway, Nat. Med. 17 (1) (2011) 64–70.
[44] Y. Su, et al., The regulatory role of PDE4B in the progression of inflammatory function study, Front. Pharmacol. 13 (2022) 982130.
[45] L.P. Tavares, et al., Blame the signaling: role of cAMP for the resolution of inflammation, Pharmacol. Res. 159 (2020) 105030.
[46] P.J. Murray, et al., Macrophage activation and polarization: nomenclature and experimental guidelines, Immunity 41 (1) (2014) 14–20.
[47] C. Zhou, et al., TRAF6 promotes IL-4-induced M2 macrophage activation by stabilizing STAT6, Mol. Immunol. 127 (2020) 223–229.
[48] J.M. Jiménez-Morales, et al., MicroRNA delivery systems in glioma therapy and perspectives: a systematic review, J. Contr. Release 349 (2022) 712–730.
[49] S. Li, et al., Payload distribution and capacity of mRNA lipid nanoparticles, Nat. Commun. 13 (1) (2022) 5561.
[50] Y. Jiang, et al., Tumor-activated IL-2 mRNA delivered by lipid nanoparticles for cancer immunotherapy, J. Contr. Release 368 (2024) 663–675.
[51] K. Mrksich, M.S. Padilla, M.J. Mitchell, Breaking the final barrier: evolution of cationic and ionizable lipid structure in lipid nanoparticles to escape the endosome, Adv. Drug Deliv. Rev. 214 (2024) 115446.
[52] J.K.W. Lam, et al., siRNA versus miRNA as therapeutics for gene silencing, Mol. ther. Nucleic Acids 4 (9) (2015) e252.
[53] S. Meulewaeter, et al., Alpha-galactosylceramide improves the potency of mRNA LNP vaccines against cancer and intracellular bacteria, J. Contr. Release 370 (2024) 379–391.
[54] H. Parhiz, et al., Added to pre-existing inflammation, mRNA-lipid nanoparticles induce inflammation exacerbation (IE), J. Contr. Release 344 (2022) 50–61.
[55] T. Ye, et al., CO-DELIVERY of glutamic acid-extended peptide antigen and imidazoquinoline TLR7/8 agonist via ionizable lipid nanoparticles induces protective anti-tumor immunity, Biomaterials 311 (2024) 122693.
[56] H. Akita, Development of an SS-cleavable pH-activated lipid-like material (ssPalm) as a nucleic acid delivery device, Biol. Pharmaceut. Bull. 43 (11) (2020) 1617–1625.
[57] K.J. Hassett, et al., Optimization of lipid nanoparticles for intramuscular administration of mRNA vaccines, Mol. ther.. Nucleic Acids 15 (2019).
[58] P. Sharma, et al., The immunostimulatory nature of mRNA lipid nanoparticles, Adv. Drug Deliv. Rev. 205 (2024) 115175.
[59] S. Omo-Lamai, et al., Lipid nanoparticle-associated inflammation is triggered by sensing of endosomal damage: engineering endosomal escape without side effects, bioRxiv (2024).
[60] S.M. Lee, et al., A systematic study of unsaturation in lipid nanoparticles leads to improved mRNA transfection in vivo, Angew. Chem. 60 (11) (2021) 5848–5853.
[61] H. Tanaka, et al., The delivery of mRNA to colon inflammatory lesions by lipid-nano-particles containing environmentally-sensitive lipid-like materials with oleic acid scaffolds, Heliyon 4 (12) (2018) e00959.
[62] Z. Zhong, et al., Lipid nanoparticle delivery alters the adjuvanticity of the TLR9 agonist CpG by innate immune activation in lymphoid tissue, Adv. Healthcare Mater. 12 (32) (2023) e2301687.
[63] L. Zhang, et al., Role of PEGylated lipid in lipid nanoparticle formulation for in vitro and in vivo delivery of mRNA vaccines, J. Contr. Release 380 (2025) 108–124.
[64] C. Wang, et al., Blood-brain-barrier-crossing lipid nanoparticles for mRNA delivery to the central nervous system, Nat. Mater. (2025).
[65] M.A. Maier, et al., Biodegradable lipids enabling rapidly eliminated lipid nanoparticles for systemic delivery of RNAi therapeutics, Mol. Ther. 21 (8) (2013) 1570–1578.
[66] X.-R. Gu, et al., Layer-by-Layer assembly of renal-targeted polymeric nanoparticles for robust arginase-2 knockdown and contrast-induced acute kidney injury prevention, Adv. Healthcare Mater. 13 (20) (2024) e2304675.
[67] K.A. Kigerl, et al., Identification of two distinct macrophage subsets with divergent effects causing either neurotoxicity or regeneration in the injured mouse spinal cord, J. Neurosci. 29 (43) (2009) 13435–13444.
[68] K. Huang, et al., Immunomodulation of MiRNA-223-based nanoplatform for targeted therapy in retinopathy of prematurity, J. Contr. Release 350 (2022) 789–802.
[69] M.S. Alqahtani, et al., Synthesis and bioactivity of a novel surfactin-based lipopeptide for mRNA delivery, Nanoscale Adv. 6 (20) (2024) 5193–5206.
[70] Y. Lee, et al., Immunogenicity of lipid nanoparticles and its impact on the efficacy of mRNA vaccines and therapeutics, Exp. Mol. Med. 55 (10) (2023) 2085–2096.
[71] S. Abbasi, S. Uchida, Multifunctional immunoadjuvants for use in minimalist nucleic acid vaccines, Pharmaceutics 13 (5) (2021).
[72] S.P. Chen, A.K. Blakney, Immune response to the components of lipid nanoparticles for ribonucleic acid therapeutics, Curr. Opin. Biotechnol. 85 (2024) 103049.
[73] N. Chaudhary, et al., Amine headgroups in ionizable lipids drive immune responses to lipid nanoparticles by binding to the receptors TLR4 and CD1d, Nat. Biomed. Eng. (2024).
[74] R.L. Rungta, et al., Lipid nanoparticle Delivery of siRNA to silence neuronal gene expression in the brain, Mol. ther.. Nucleic Acids 2 (12) (2013) e136.
[75] H. Tanaka, et al., In vivo introduction of mRNA encapsulated in lipid nanoparticles to brain neuronal cells and astrocytes via intracerebroventricular administration, Mol. Pharm. 15 (5) (2018) 2060–2067.